MODIFYING HIGH-ORDER AEROELASTIC MATH MODEL OF A JET TRANSPORT USING MAXIMUM LIKELIHOOD ESTIMATION

By

Amir A. Anissipour and Russell A. Benson
The Boeing Company
Seattle, Washington

ABSTRACT

The design of control laws to damp flexible structural modes requires accurate math models. Unlike the design of control laws for rigid body motion (e.g., where robust control is used to compensate for modeling inaccuracies), structural mode damping usually employs narrow band notch filters. In order to obtain the required accuracy in the math model, maximum likelihood estimation technique is employed to improve the accuracy of the math model using flight data. This paper presents all phases of this methodology: (1) pre-flight analysis (i.e., optimal input signal design for flight test, sensor location determination, model reduction technique, etc.), (2) data collection and preprocessing, and (3) post-flight analysis (i.e., estimation technique and model verification). In addition, a discussion is presented herein of the software tools used for this study and the need for future study in this field.

Modifying High-Order Aeroelastic Math Model of a Jet Transport Using Maximum Likelihood Estimation

Amir A. Anissipour
Russell A. Benson

The Boeing Company
Boeing Commercial Airplanes
P.O. Box 3707 M/S 9W-38
Seattle ,Wa. 98124

ABSTRACT

The design of control laws to damp flexible structure modes requires accurate math models of the dynamic system. To obtain the required accuracy of a math model, the parameter estimation technique using maximum likelihood estimation is employed to improve the accuracy of the model based on flight data. This paper presents all phases of this methodology: pre-flight analysis (i.e., optimal input signal design for flight test, sensor location determination, model reduction technique, etc.), data collection and preprocessing, and post-flight analysis (i.e., estimation technique and model verification). The results of this study indicate that the parameter estimation technique (i.e., maximum likelihood estimation) is an effective and powerful technique in modifing high-order aeroelastic aircraft models. However, the accuracy of the results depends upon the fidelity of the theoretical model with regards to the correct number of dominant modes for the desired frequency bandwith in the model (i.e., model order). If the number of modes in the model are not representative, then an identification problem can occure in the parameter estimation technique. Nevertheless, this problem can be overcome using the system identification technique.

INTRODUCTION

Having an accurate mathematical representation is fundamental to any aircraft control system design. In general, aircraft models are developed from a theoretical basis and modified by analyzing the experimental data (i.e., wind-tunnel data for aerodynamic models or ground shake test data for structural models). Although present techniques provide very good dynamic models for the design stages of an aircraft, often these models do not match the actual dynamic flight response. This problem has generated a need for advanced system identifiaction and parameter estimation techniques in upgrading dynamic models of an aircraft based on flight test data. This modeling problem is more apparent with high-order aeroelastic models with which our experince with modeling techniques is limited.

Low-frequency structural modes are easily excited for a jet transport with a long fuselage. This excitation causes a lateral ride discomfort in certain flight conditions. In order to design a yaw damper to dampen Dutch roll response and suppress the undesirable low-frequency structure modes by means of active control, an accurate aeroelastic model of the aircraft must be available. In this study, parameter estimation technique is applied to upgrade the high-order aeroelstic math model of a jet transport. The following is a summary of the parameter estimation technique using maximum likelihood estimation.

Maximum Likelihhood Estimation

Suppose the actual system is described by (Reference 1):

$$\dot{x}(t) = A\,x(t) + B\,u(t) + S\,s(t) + F\,n(t)$$
$$z(t_i) = C\,x(t_i) + D\,u(t_i) + H\,s(t_i) + G\,m(t_i) \qquad (1)$$

where

$x(t)$	state vector
$u(t)$	control vector
$z(t_i)$	measurement vector
$s(t)$	bias vector
$n(t)$	process noise
$m(t_i)$	measurement noise
t_i	time sample
A, B, C, D, S, H, F, G	system matrices with unknown parameters

$n(t)$ and $m(t)$ are zero mean, Gaussian and independent noise

Assume k is the vector of unknowns that contains elements of the system matrices A, B, C, D, S, H, F and G. The objective is to maximize the probability distribution of unknowns (i.e., k) when the measurements z are available. Therefore, maximizing P(k/z), where P is the probability distribution function of k given z.

By Bayes' rule:

$$P(k/z)\ P(z) = P(k,z) = P(z/k)\ P(k) \tag{2}$$

or

$$P(k/z) = P(z/k)\ \frac{P(k)}{P(z)} \tag{3}$$

Since in these equations z is given, so P(z) becomes a constant. Assume there is no a priori preference for k, so P(k) becomes a constant. Therefore, P(z/k) differs from P(k/z) only by a constant. In other words equation (3) becomes:

$$P(k/z) = P(z/k) \cdot \text{constant} \tag{4}$$

Equation (4) indicates that P(z/k) may be maximized instead of P(k/z). Therefore, using Gaussian assumption, the likelihood ratio may be written as:

$$P(z/k) = \left[(2\pi)^L |GG^*|\right]^{-\frac{1}{2}N} \exp\left\{-\frac{1}{2}\sum_{i=1}^{N}\left[z_k(t_i)-z(t_i)\right]^* (GG^*)^{-1}\left[z_k(t_i)-z(t_i)\right]\right\} \tag{5}$$

where

$z_k(t_i)$	predicted estimate at time t_i
GG^*	measurement noise covariance matrix
L	number of measurements

If the logarithm of equation (5) is taken, the consatnt terms are eliminated by the maximization, and the equation is multiplied by -1 to do minimization rather than maximization, then equation (6) will be obtained as:

$$J(k) = \frac{1}{2} \sum_{i=1}^{N} \left\{ \left[z_k(t_i) - z(t_i) \right]^* (GG^*)^{-1} \left[z_k(t_i) - z(t_i) \right] \right\} \tag{6}$$

where J(k) is the cost function to be minimized. Two steps are taken to obtain $z_k(t_i)$. Prediction step:

$$\begin{aligned} x_k(t_{i+1}) &= \Phi\, x_k(t_i) + \Psi\, u(t_{i+1/2}) \\ z_k(t_{i+1}) &= C\, x_k(t_{i+1}) + D\, u(t_{i+1}) \end{aligned} \tag{7}$$

where

$$\Phi = e^{A\,\Delta t} \qquad \text{and} \qquad \Psi = \int_0^t e^{A\,s}\, ds$$

and the correction step:

$$x_k(t_{i+1}) = x_k(t_{i+1}) + K \left[z(t_{i+1}) - z_k(t_{i+1}) \right] \tag{8}$$

K in equation (8) is the Kalman filter gain matrix given by:

$$K = P\, C^* (GG^*)^{-1} \tag{9}$$

where P is the solution to the discrete time Riccati equation:

$$A\,P + P\,A^* - \frac{1}{\Delta t} P C^* (GG^*)^{-1} C\,P + F F^* = 0 \tag{10}$$

After obtaining the cost function J(k), the Newton-Raphson algorithm is used iteratively to minimize the cost function by revising the unknowns parameters.

$$k_{i+1} = k_i - \left\{ \nabla_k^2 J(k_i) \right\}^{-1} \left\{ \nabla_k^* J(k_i) \right\} \tag{11}$$

This algorithm requires an intial estimate for the vector of unknowns (k_0). A priori estimate is available for each unknown parameter through the analytical model.

The MMLE software tool developed by NASA Dryden is a parameter estimation program supporting this estimation technique. This software has been modified by Boeing to accept and handle higher order models. A comprehensive description of this software tool is described in Reference 1.

PRE-FLIGHT ANALYSIS

Math Model

A sixtieth order linear aeroelastic math model for a flight condition of Mach .6 speed, 15000 foot altitude, and no turbulance, and cruise configuration of a jet transport was provided in the form of:

$$M\ddot{q} + C\dot{q} + Kq = u \tag{12}$$

where
- M mass matrix
- C damping matrix
- K stiffness matrix
- q generalized coordinate
- u control inputs

The model is defined in the inertial axis system, and the dynamics (q), consist of rigid body and flexible modes. The model is tuned using data from ground shake testing. The system of equations (12) was transformed into state-space form using the following transformation:

$$X_m = \begin{bmatrix} q \\ \dot{q} \end{bmatrix}$$

therefore the system equation (12) becomes:

$$\dot{x} = A_m x_m + B_m u$$
$$y = C_m x_m + D_m u \qquad (13)$$

where

$$A_m = \begin{bmatrix} 0 & I \\ -M^{-1}K & -M^{-1}C \end{bmatrix}$$

and

$$B_m = \begin{bmatrix} 0 \\ M^{-1} \end{bmatrix}$$

This transformation always exists because the mass matrix is positive definite. Although this is a well-posed theoretical problem, it is not trivial. The flexible model is usually on the order of one hundred states, thus causing numerical inaccuracies in the inversion of the mass matrix. In our analysis the software package MPAC was used to perform the transformation. (MPAC is a numerically robust modern control and analysis software tool developed by the Boeing Company.)

For the identification process, the system equation (13) was transformed into the conjugate modal form using the following transformation:

$$m = T^{-1} x_m$$

Equation (13) becomes:

$$\dot{m} = \Lambda m + \bar{B} u$$
$$y = \bar{C} m + D u \qquad (14)$$

where

$\Lambda = \text{dia}\,(\lambda_i)$ $\quad\quad$ $\lambda_i = i^{th}$ eigenvalue

$\bar{B} = T^{-1} B$ $\quad\quad$ controllability matrix

$\bar{C} = C\,T$ $\quad\quad$ observability matrix

The advantage of using the modalized form given by equation (14) is that all the modes through Λ matrix, along with the controllability and observability matrices are readily available for an analyst to quickly locate uncontrollable and unobservable modes. In addition, the modes in the Λ matrix are decoupled and may be partitioned into rigid model and elaastic model.

The order of the model was reduced to nineteen by deleting the modes above 6 Hz. Since this model will eventually be used for ride quality study and modal supperasion design, only those modes less than 6 Hz were retained.

The reduced order, modal model (19th order) is represented by:

$$\begin{aligned} \dot{m}_r &= \Lambda_r\, m_r + \bar{B}_r\, u \\ y &= \bar{C}_r\, m_r + D_r\, u \end{aligned} \qquad (15)$$

This model contains one state for heading, one for the spiral mode, two for the Dutch roll mode, one for roll mode, eight for low-damped elastic modes, and six for high-damped elastic modes.

To support this study, a special set of sensors were installed on the aircraft to measure the dynamic response of the jet transport. The locations of these sensors were based on the mode shapes of the aircraft determined by the math model and physical constraints (Table I). (A complete discussion on sensor selection and location placement on the aircraft is omitted herein for proprietary reasons.)

TABLE I: Sensor Type and Locations for High-order Aeroelastic Modeling

SENSOR TYPE	SENSOR LOCATION
Position Transducer	On all control surfaces
Yaw Rate Gyro	Pilot seat, IRU (a station between CG and cockpit below the cabin floor), CG station
Lateral Accelerometer	1 Pilot seat, 1 Cockpit ceiling, 8 on the passanger cabin floor from the cockpit to the aft galley, 1 on the aft galley ceiling, 3 on vertical tail (tip and mid section, front and rear spar), three on each nacelle, 1 IRU station
Vertical Accelerometer	1 on the pilot seat, 1 IRU, 1 aft galley, 8 on each wing, 3 on each horizontal tail, 2 on each nacelle
Roll rate, Yaw rate, Bank angle, Heading,	IRU and CG stations

The sensors selected for the analysis were: body roll angle (Φ), heading angle (Ψ), roll rate (p) and yaw rate (r) at the IRU; body yaw rate at the pilot seat; 9 lateral accelerometers along the fuselage; 2 lateral accelerometers on the nacelle number 2; and 3 lateral accelerometers on the vertical tail.

Input Signal Design

The flight test input-signal design analysis for high-order aeroelastic modeling was performed using the reduced order analytical model (equation 15). Although a number of "optimum" input signals have been proposed for flight testing in conjunction with parameter estimation, none have been found to be appropriate for

high-order aeroelastic modeling. Essentially, all the analytical techniques proposed in designing the optimum input signals are based on the analytical model. This model is the subject of improvement by the identification and estimation techniques. Hence, no "optimum" input signal exists.

A number of different input signals were evaluated for this study. After a comprehensive simulation study, it was determined that a frequency sweep of a linear sine-wave with adequate energy to excite all the modes (rigid and elastic) yeilds the best results. In addition, the linear sine-wave frequency sweep optimizes the most commonly used criterion for input signal design:

$$\Re = -\log\ (\det M) \tag{16}$$

where M is the Fisher information matrix (or sensitivity matrix) defined by:

$$M = \nabla_k^2 J(k) \tag{17}$$

J is the cost function defined in equation (6). The criterion $\Re$ defined in equation (16) is related to the volume of highest probability density region for the parameters k. An interesting property of the determinant criterion is that it is independent of scaling parameters (Refernce 2).

Fifteen tests were designed for the same flight condition. Five frequency sweeps were designed for each control surface. Each test was repeated for rudder, aileron, and both surfaces in phase. The first frequency sweep covered 0 to 6 Hz to excite all the modes in one test. The other four tests were then designed to excite specifically high-damped modes by sweeping from .25 Hz below to .25 Hz above the frequency of the mode.

The amplitude of the input signals were designed to be constant for practical purposes (i.e., rate limits). The designed input signals were tested in the lab to confirm that the signals did not saturate the servos and actuators of the control surfaces. However, the output of the actuators during flight test generated signals with decaying amplitutes. These decaying amplitudes reduced the energy level initially designed for the test. Figures 1 and 2 show the actual control surface

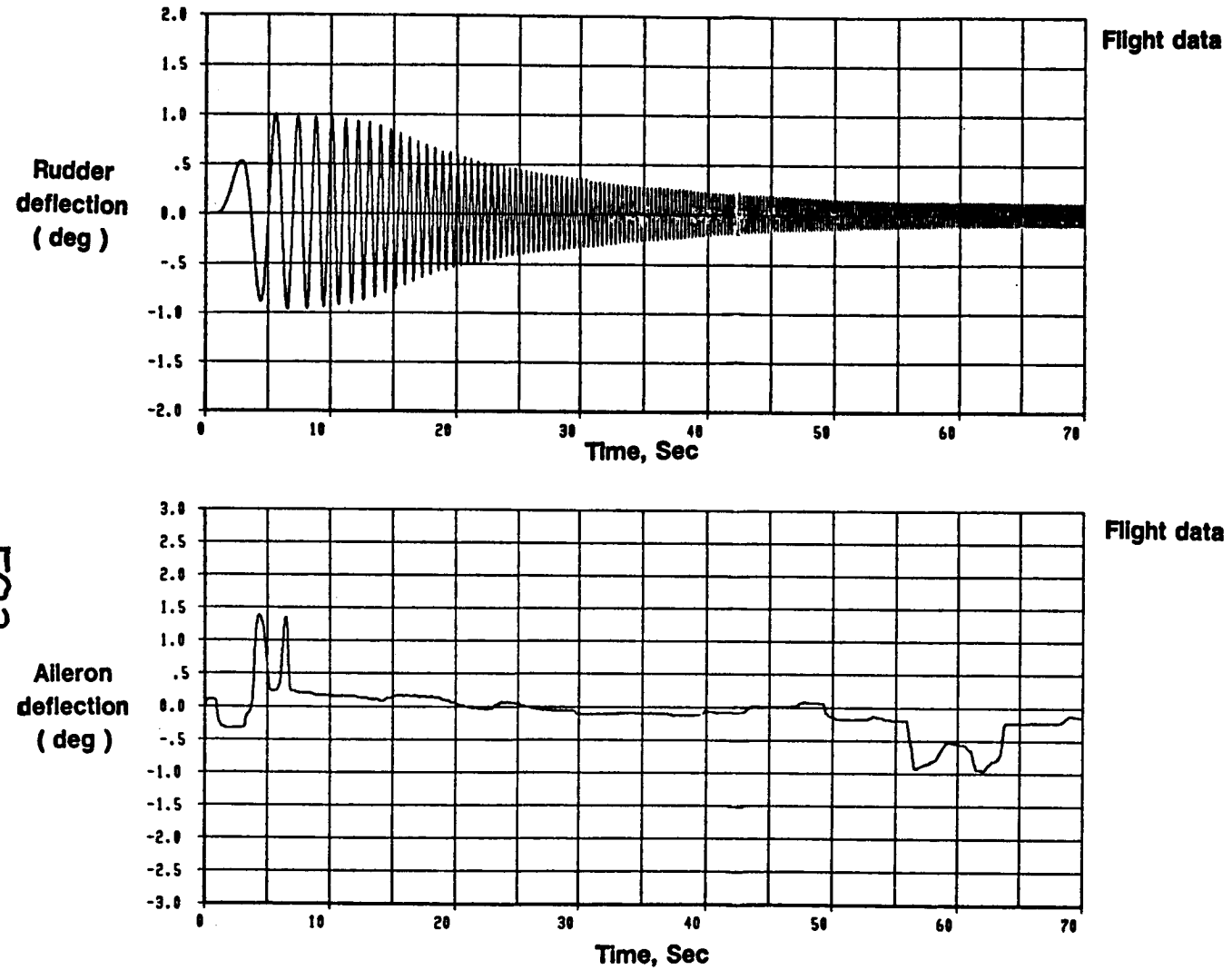

Figure 1. Actual Control Surface Deflections for Flight Condition 21

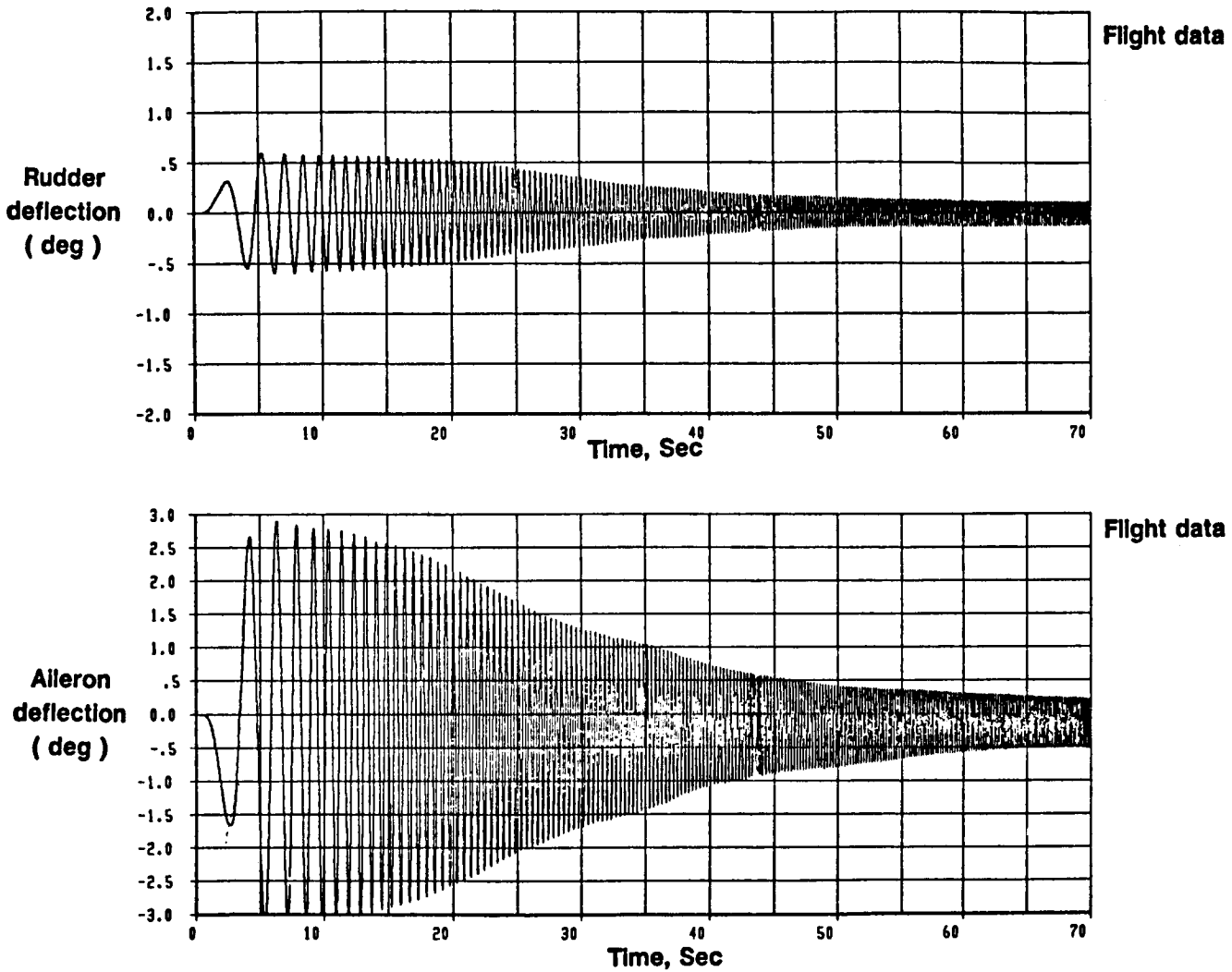

Figure 2. Actual Control Surface Deflections for Flight Condition 41

deflections for rudder sweep alone, and for rudder and aileron surfaces simultaneously in phase.

Sampling Frequency

To record the data in flight test, a simulation study was conducted to determine the required sampling frequency. The analytical model (i.e., system equations 15) was assumed to be the true model, and simulated using the designed input signal. A considerable amount of noise was added to the simulation data, and then that data was treated as pseudo-flight data. The acutal model was used for parameter estimation to determine the required sampling frequency. Sampling frequencies of 20, 25, 50, 100, 200 Hz were considered for this study. One mode or group of modes at a time were selected for the estimation process of each sampling frequency. The results indicated that 100 Hz is the best sampling frequency for this study. Figure 3 shows the typical results for identified parameters when different sampling frequencies were used.

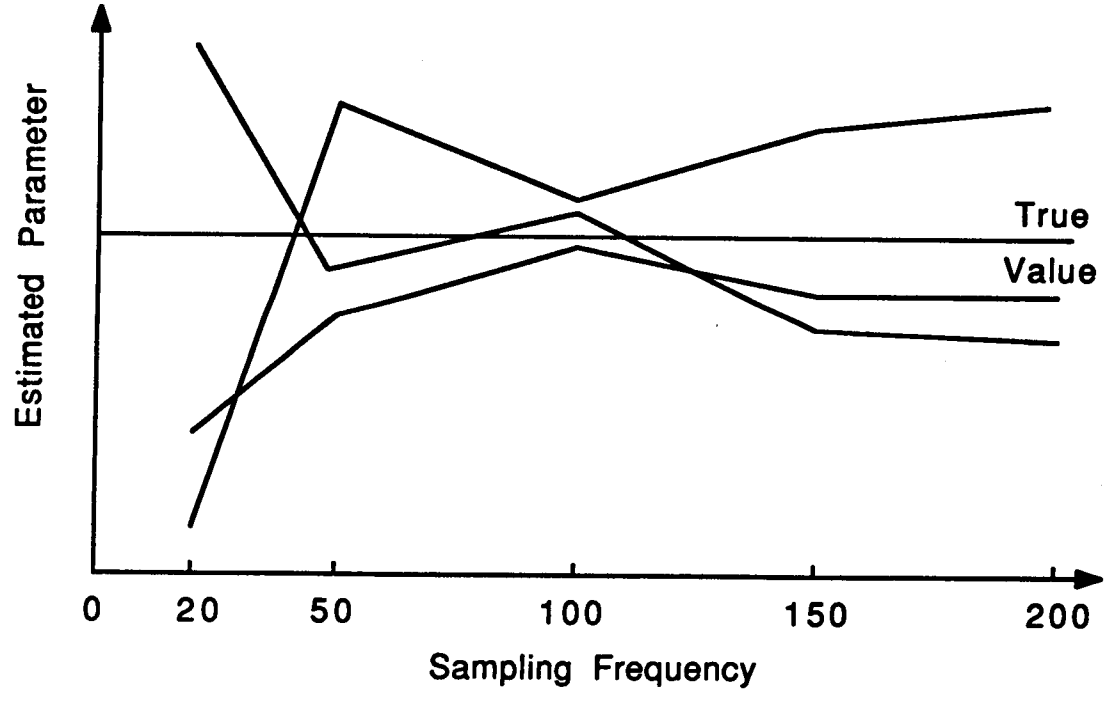

Figure 3. Typical Results from Estimation with Different Sampling Frequency

FLIGHT TEST

The flight test was performed using designed linear sine-wave frequency sweeps for rudder and aileron. The test conditions were conducted at a speed of Mach .6, an altitude of 15,000 feet, and minimal turbulence. A preprogrammed frequency function generator was used to apply the linear sinusoidal frequency sweeps (0-6 Hz) to the aileron and rudder (through the autopilot servo).

The flight test data were recorded with 100 sample per second, and then filtered using a Graham low-pass filter with the cutoff frequency of 10 Hz and rolloff frequency of 15 Hz. Prior to estimation analysis, the data were cleaned up by removing all the sensor biases and data dropouts.

POST FLIGHT ANALYSIS

The analytical model (system equations 15) was simulated using actual control surface defelection during flight as input signals. The comparison of flight data with the response of the analytical model for flight condition 41, where both rudder and aileron frequency sweeps are used, is presented in the Figures 4-11.

The maximum likelihood estimation software tool (MMLE) developed by NASA Dryden was used to minimize the residuals between flight data and response of the analytical model in Figures 4-11. At the time of analysis, MMLE was hosted on the Cyber mainfram. Due to Cyber having a memory limit, the capability of using process noise was not available for analysis. Hence the results obtained herein, are preliminary results which do not include the effect of process noise. The final results of this study will be reported at the 1989 AIAA Guidance, Navigation and Control conference.

The high-order model was partitioned into two sections: rigid model and elastic model. For rigid model identification, 15 seconds of data were used. First the rigid portion of the control and measurement matrices were upgraded. Then, the Λ matrix was upgraded. Finally, all the parameters in the rigid section of the $\Lambda, \bar{B}$ and $\bar{C}$ matrices were simultaneously estimated.

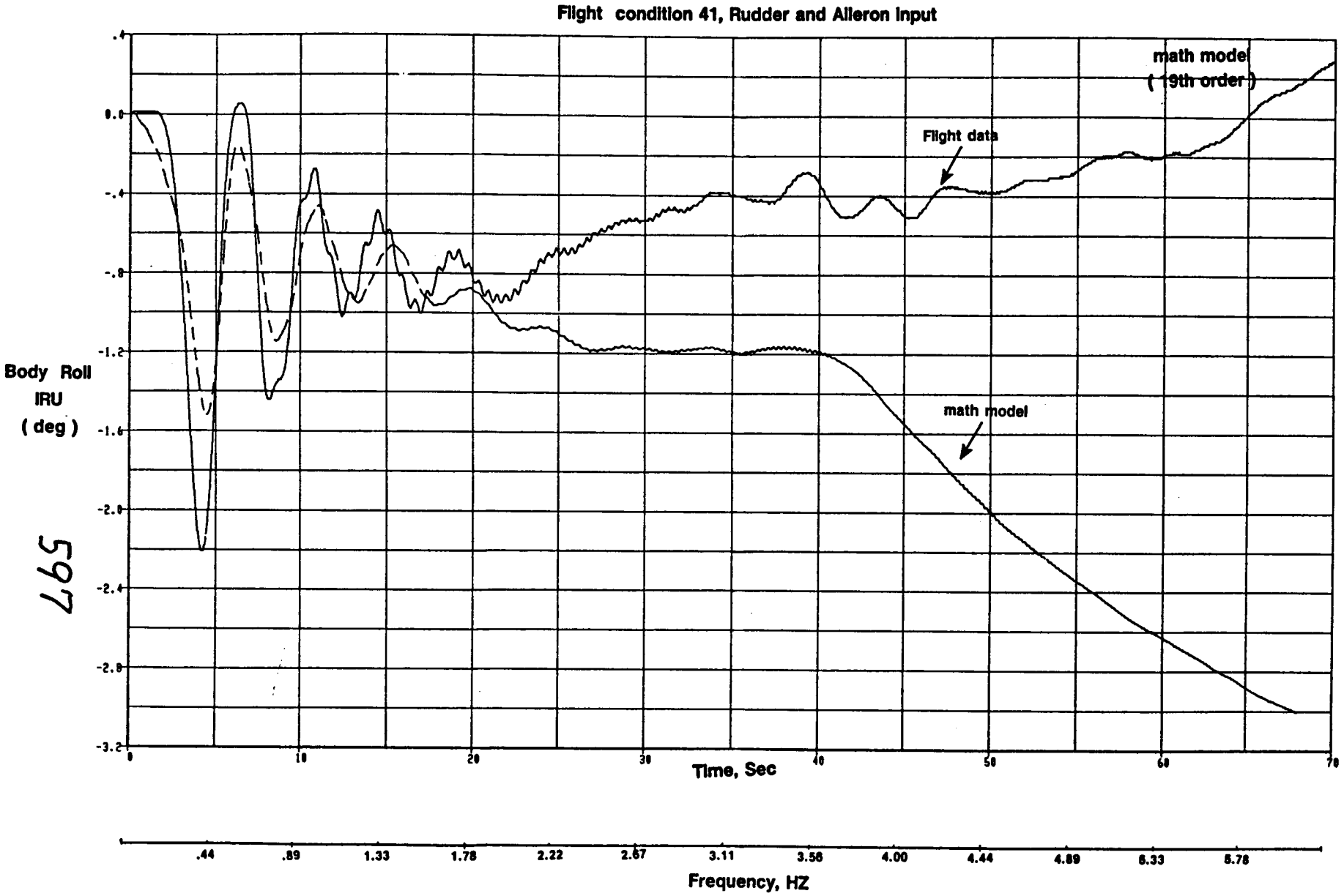

Figure 4. Time Response of Body Roll at IRU Comparing Flight Data with Math Model

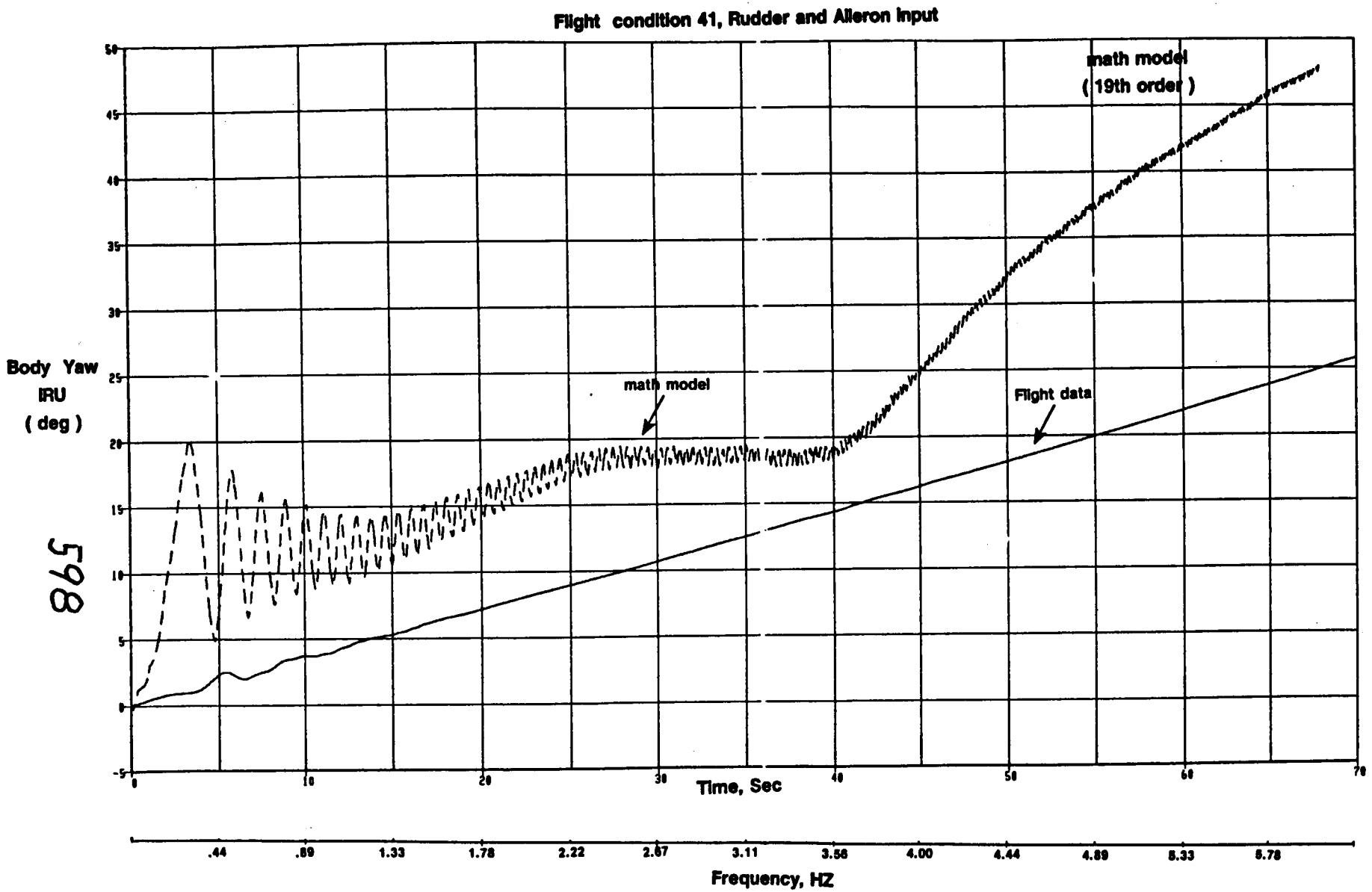

Figure 5. Time Response of Body Yaw at IRU Comparing Flight Data with Math Model

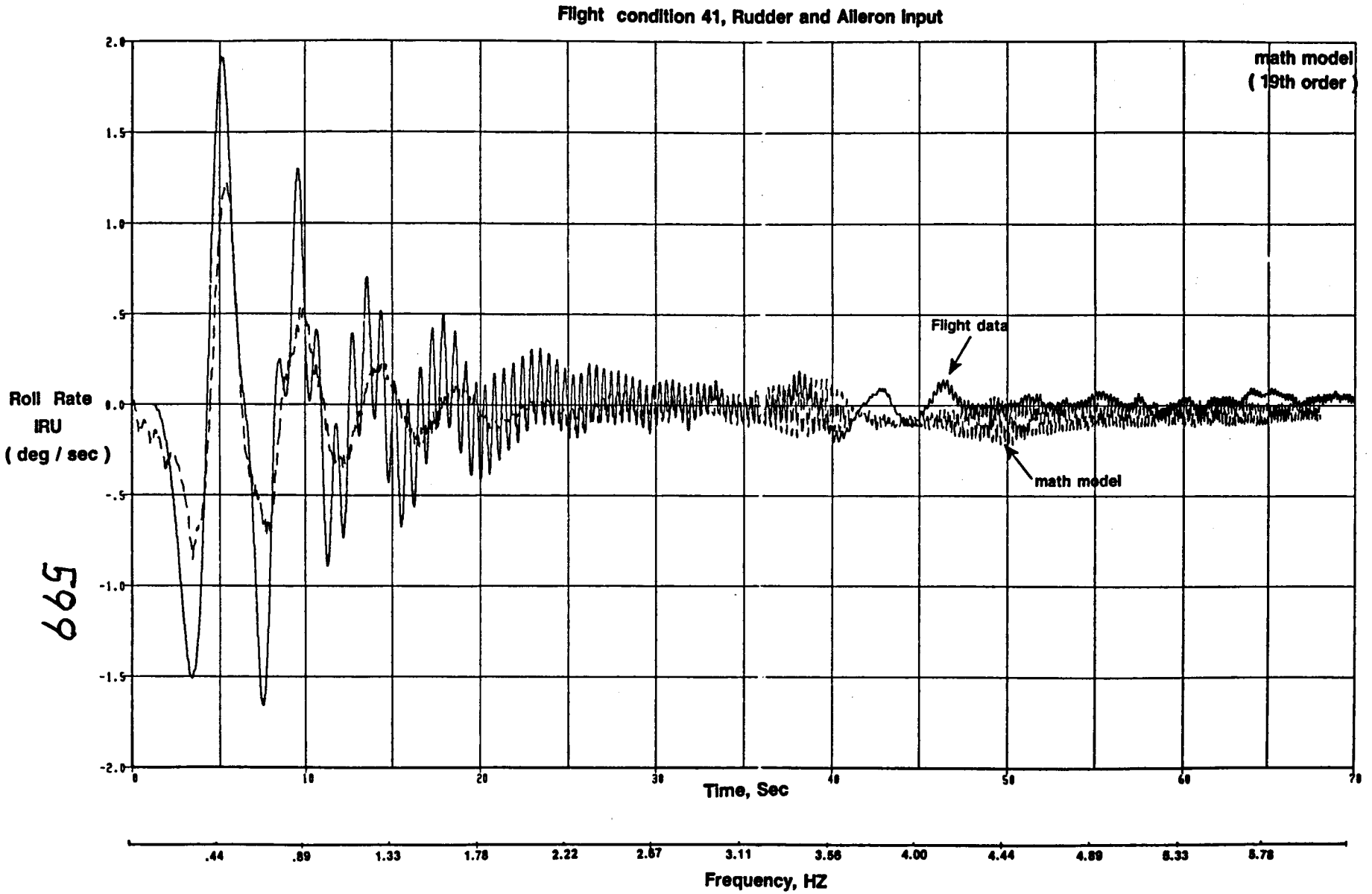

669

Figure 6. Time Response of Roll Rate at IRU Comparing Flight Data with Math Model

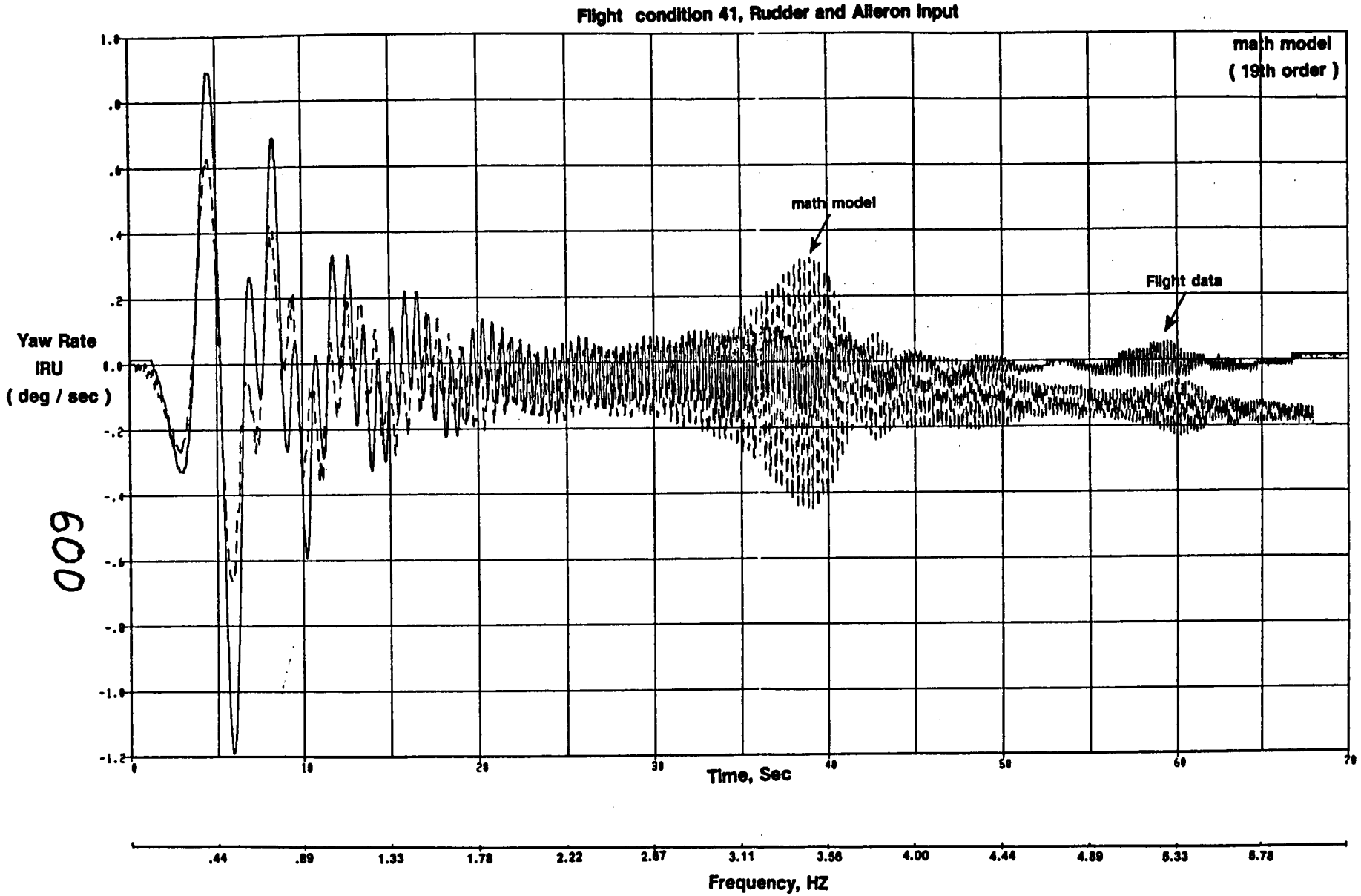

Figure 7. Time Response of Yaw Rate at IRU Comparing Flight Data with Math Model

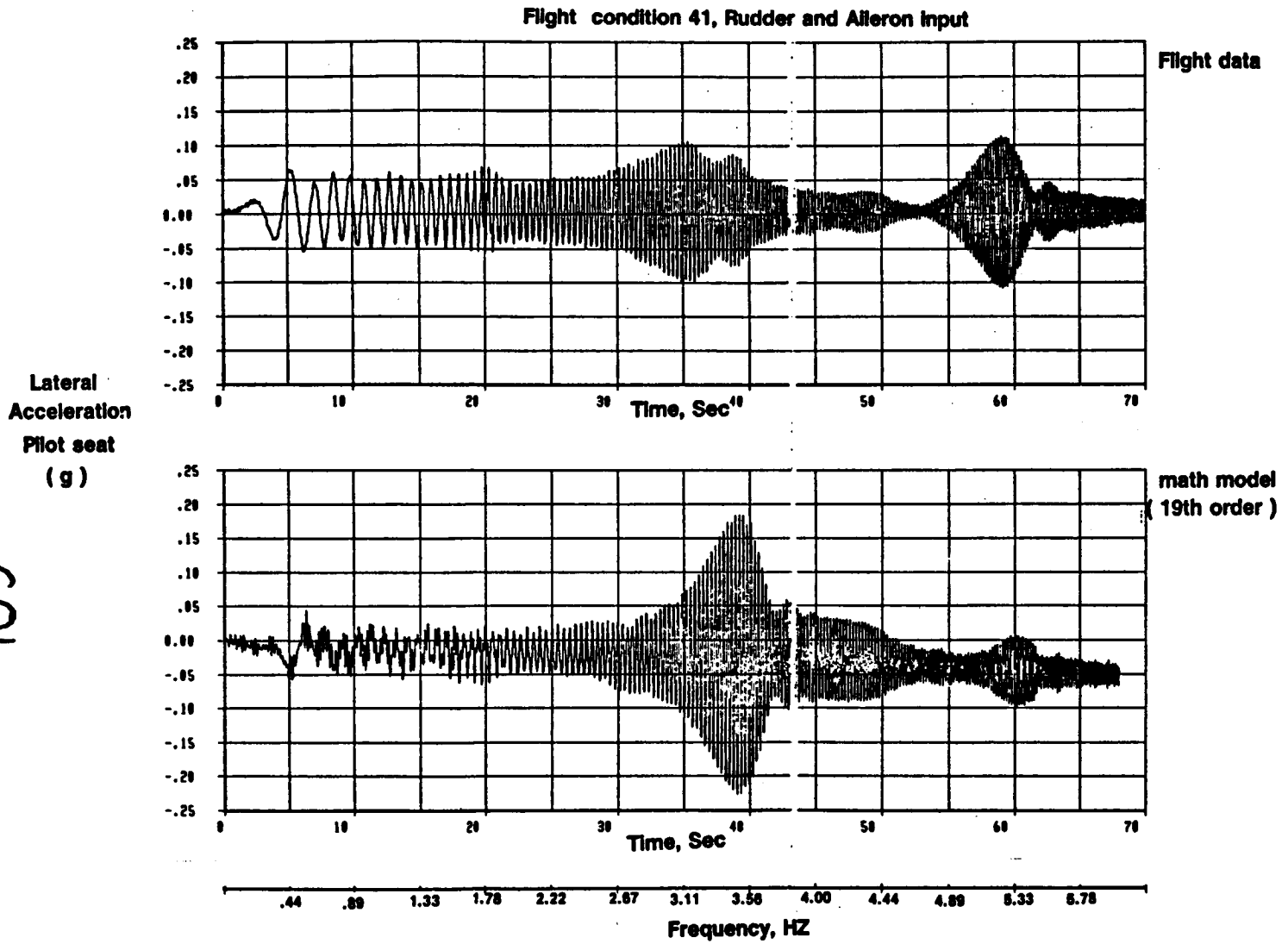

Figure 8. Time Response of Lateral Acceleration at Pilot Seat Comparing Flight Data with Math Model

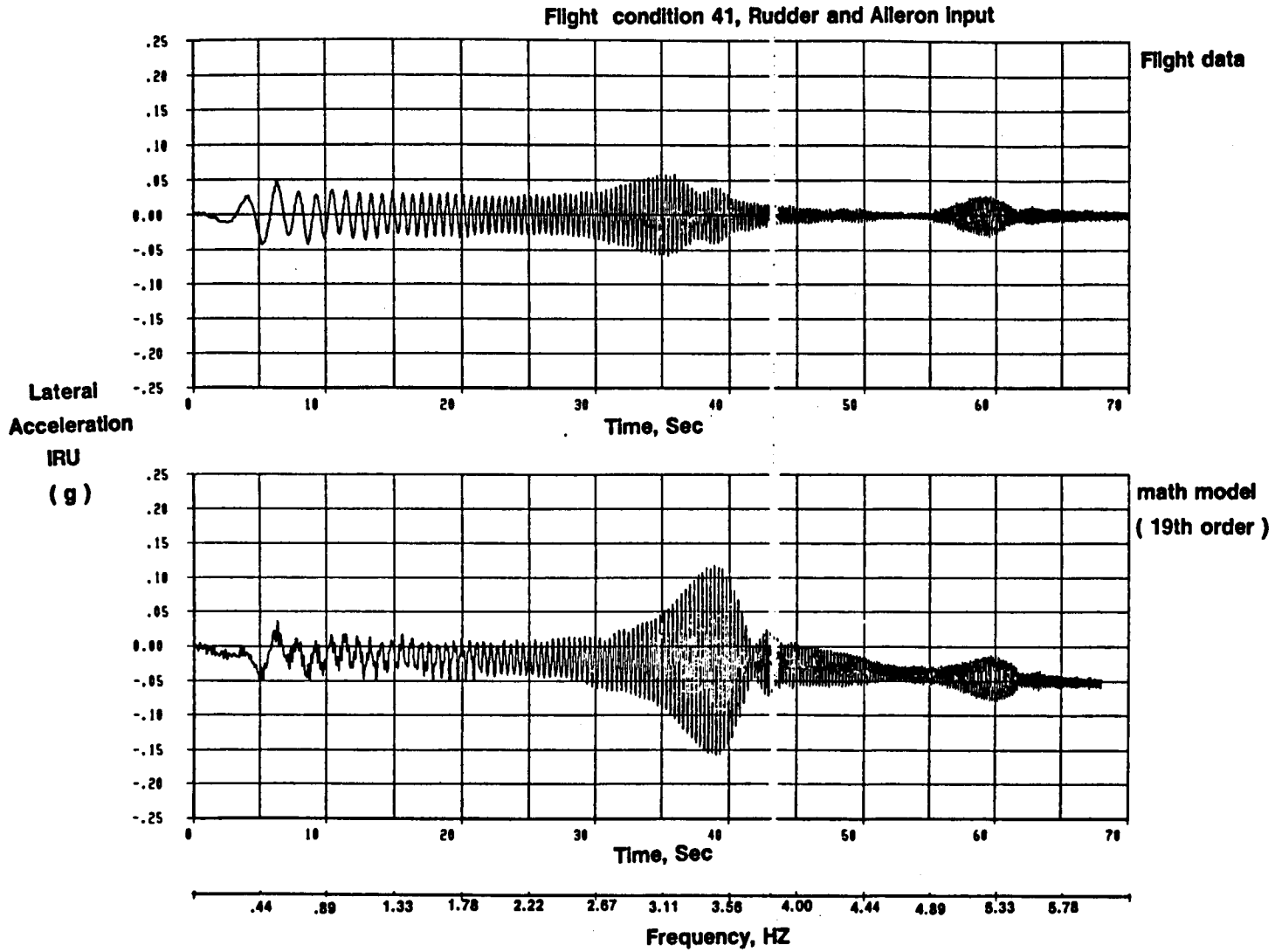

Figure 9. Time Response of Lateral Acceleration at IRU Comparing Flight Data with Math Model

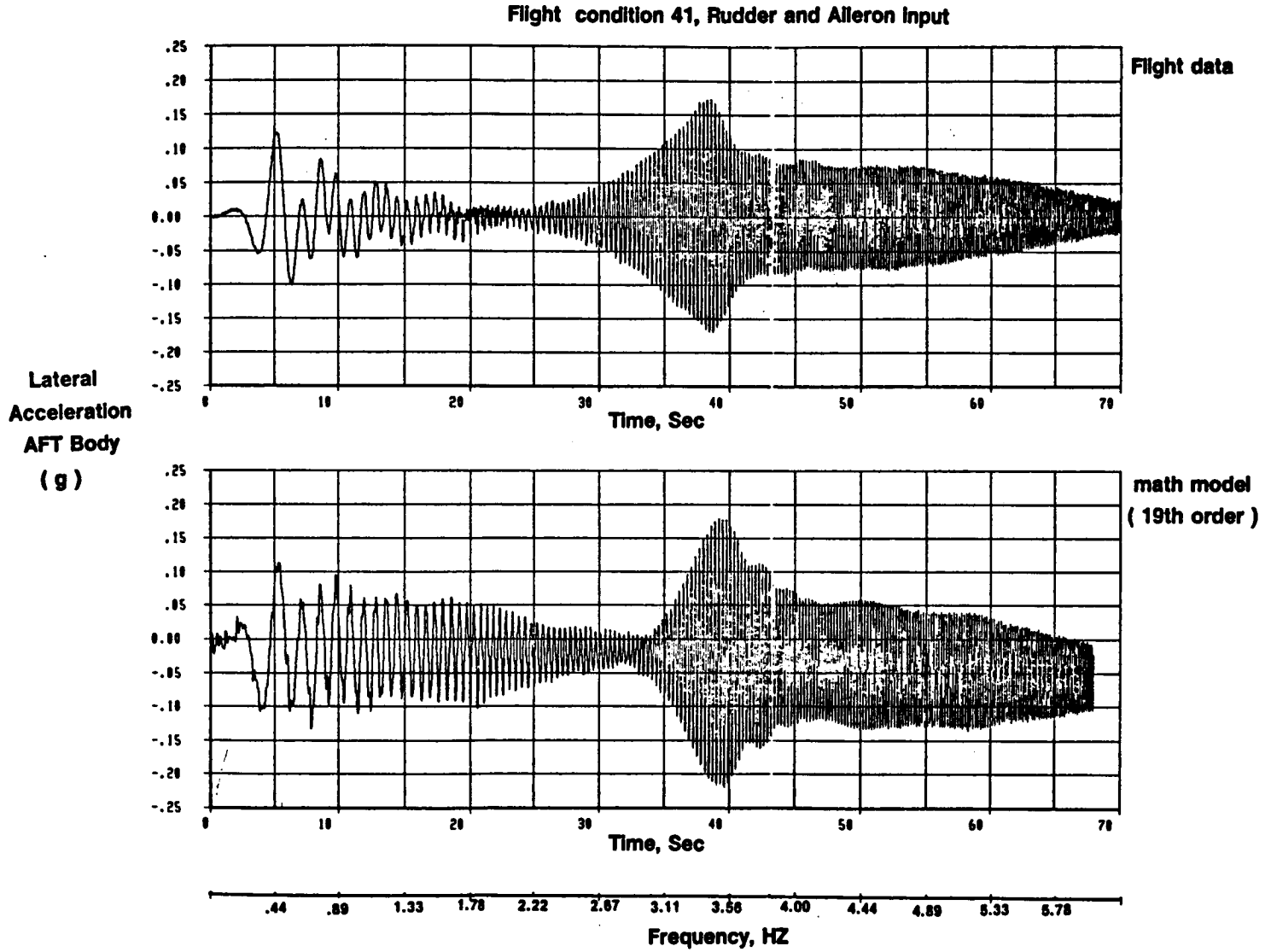

603

Figure 10. Time Response of Lateral Acceleration at AFT Body Comparing Flight Data with Math Model

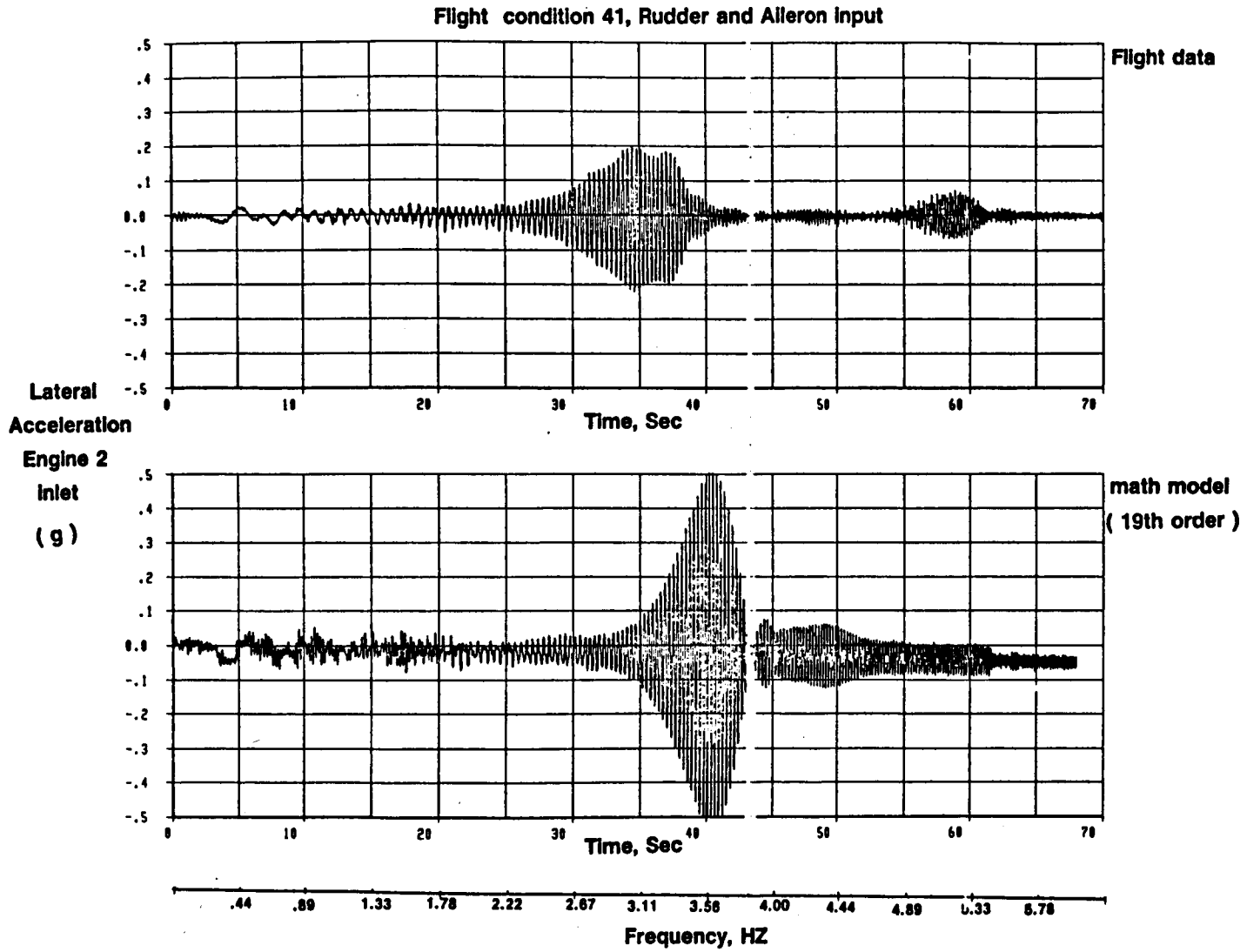

Figure 11. Time Response of Lateral Acceleration at Engine 2 Inlet Comparing Flight Data with Math Model

Two different approches were taken for the elastic model identification. In the first approach, the 19th order model was used for the analysis with all the elements of $\bar{B}$ and $\bar{C}$ being estimated. All 70 seconds of data were used for this estimation approach, . In this process, those parameters in the $\bar{B}$ and $\bar{C}$ that did not contribute to the residuals were identified and kept constant for the remainder of the analysis. Then, the elements of Λ were added to the estimation process while keeping some of the elements of $\bar{B}$ and $\bar{C}$ constant. The results of this estimation approach are show in Figures 12-19.

The second approach was to add one elastic mode at a time to the rigid model. For this approach, the first elastic mode was added with 28 seconds of data used for the analysis. The corresponding parameters in the $\bar{B}$ and $\bar{C}$ matrices were estimated every time a mode was added to the model. The result of this approach was not satisfactory because several times the algorithem diverged and the residuals were big.

Figures 20-26 show the PSD plots obtained from the analytical model. Figures 27-34 show the PSD plots obtained from the estimated model. The PSD plots obtained from the estimated model, clearly show that the estimation analysis improved the accuracy of the model in terms of its modal representation. However, the estimated parameters in the $\bar{B}$ and $\bar{C}$ matrices are biased. Since an accurate representation of the transfer functions was desired for this study rather than true values of the $\bar{B}$ and $\bar{C}$ matrices, the biased estimates in the $\bar{B}$ and $\bar{C}$ matrices did not create any problem.

Figures 16, 17 and 19 indicate that another mode is present in the flight data which is not modeled in the analytical or estimated model. This problem can not be solved via parameter estimation technique which assumes the structure of the model (i.e., the order of the model) is correct. Hence, it is suggested that the system identification technique developed by V. klein and J. Batterson of NASA LaRC be used to overcome this problem.

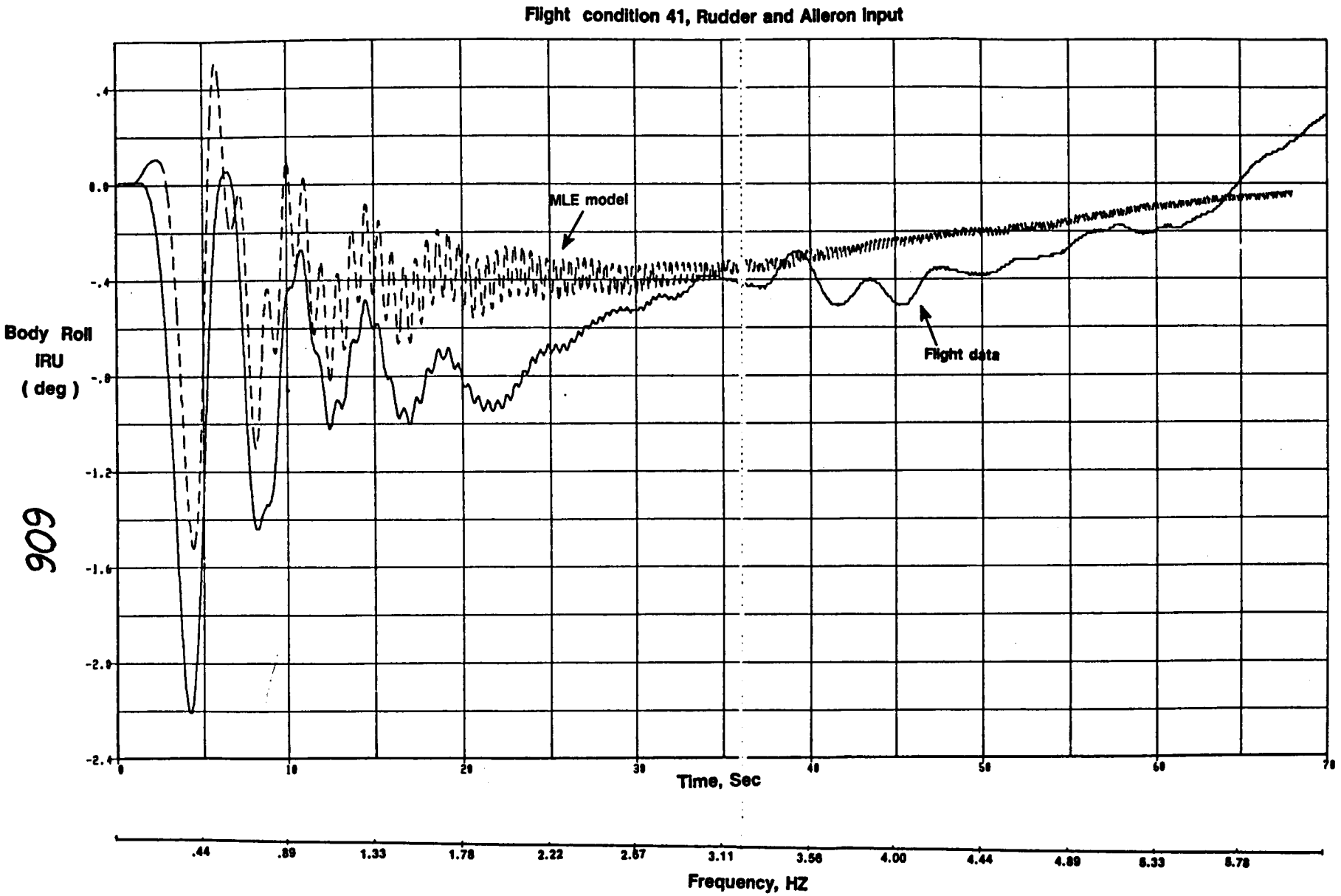

909

Figure 12. Time Response of Body Roll at IRU Comparing Flight Data with MLE Model

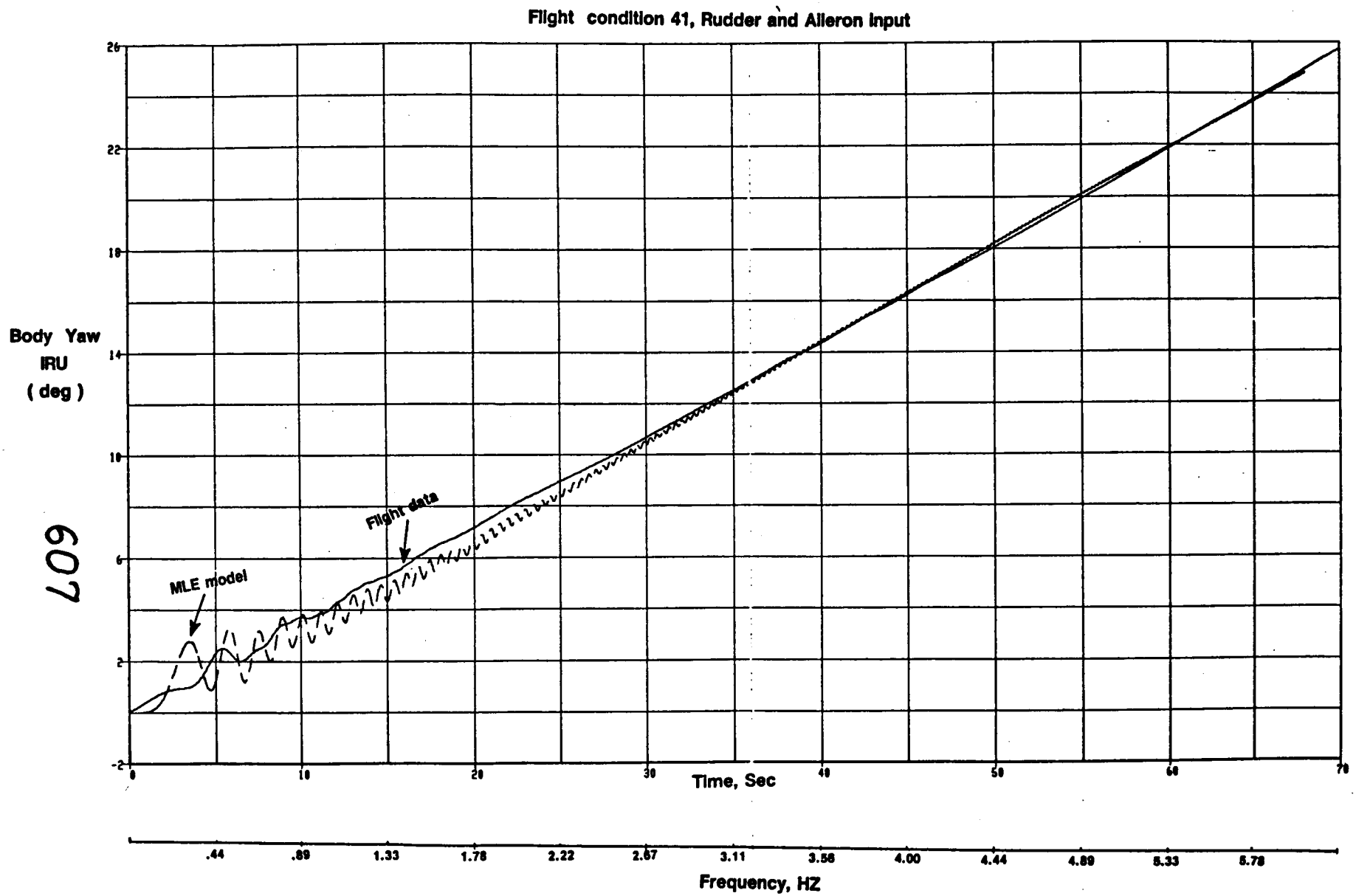

607

Figure 13. Time Response of Body Yaw at IRU Comparing Flight Data with MLE Model

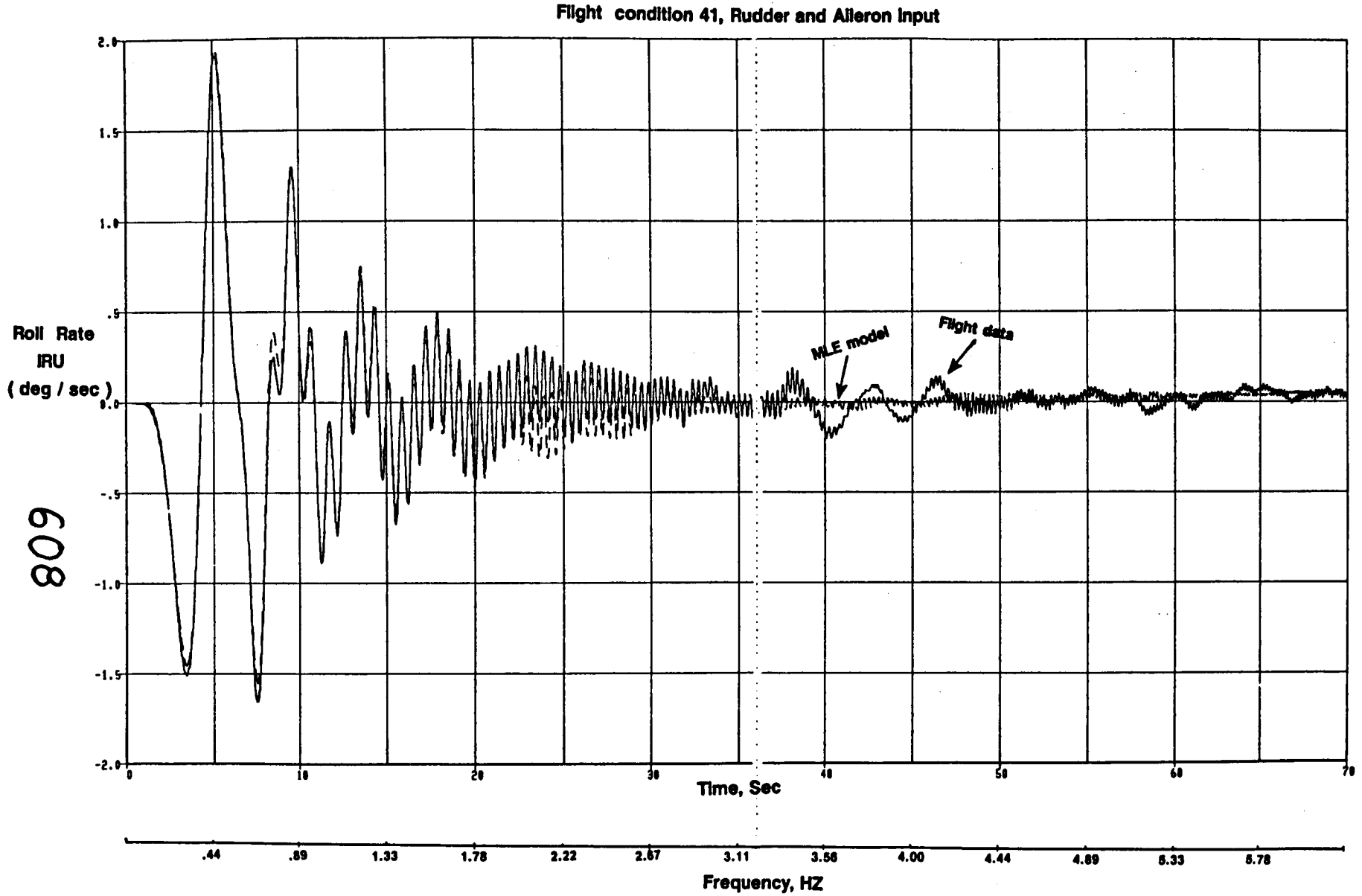

Figure 14. Time Response of Roll Rate at IRU Comparing Flight Data with MLE Model

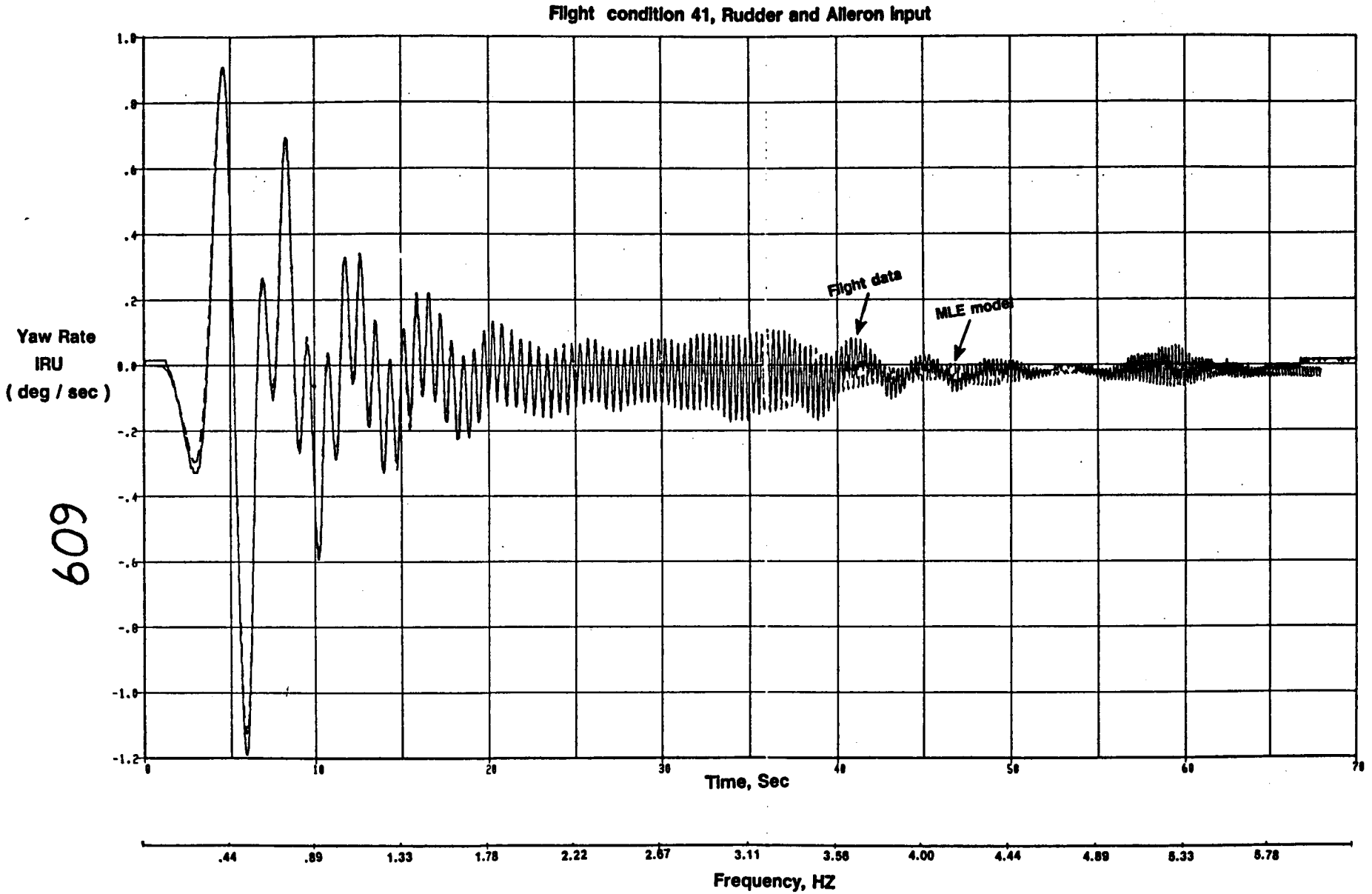

609

Figure 15. Time Response of Yaw Rate at IRU Comparing Flight Data with MLE Model

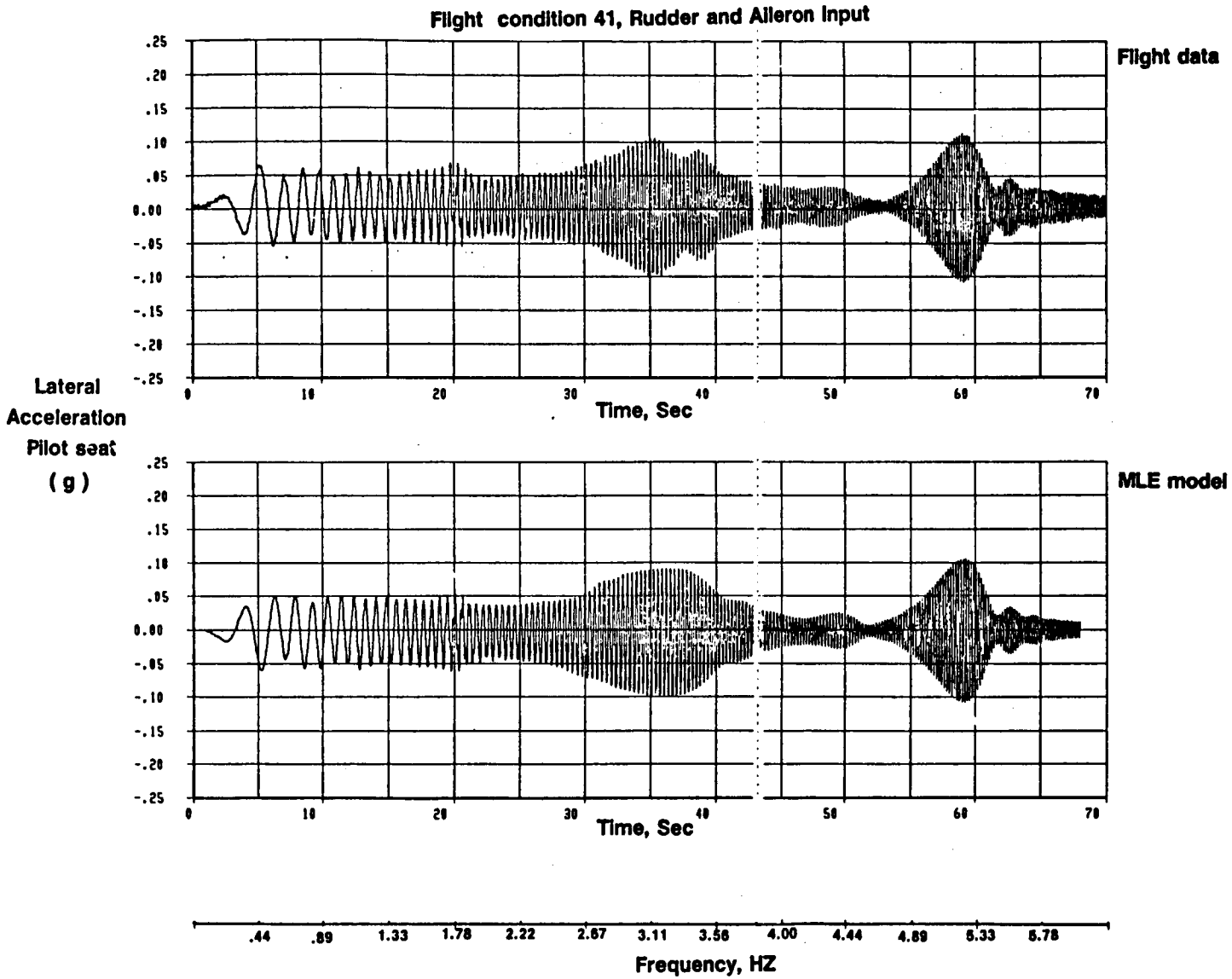

Figure 16. Time Response of Lateral Acceleration at Pilot Seat Comparing Flight Data with MLE Model

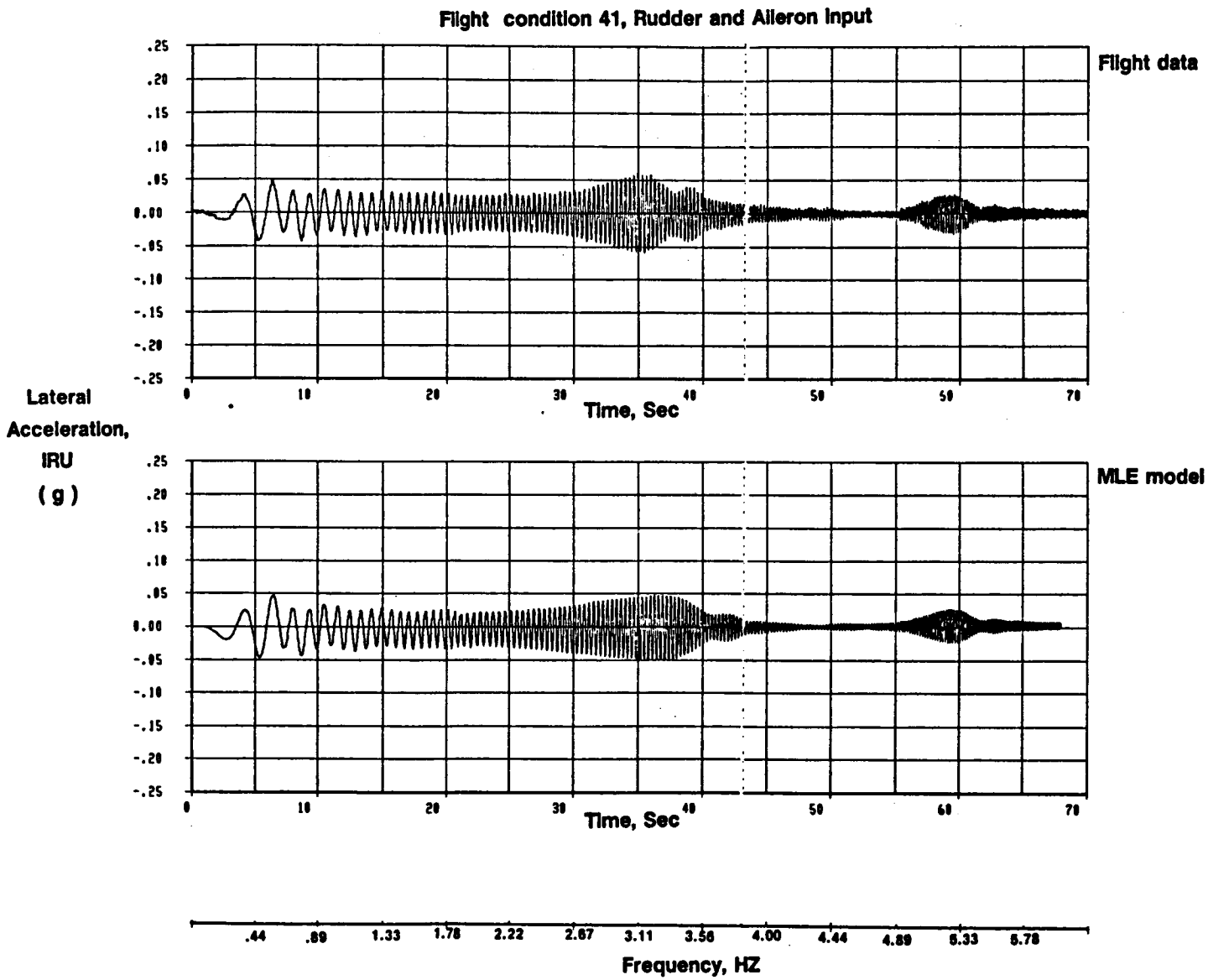

Figure 17. Time Response of Lateral Acceleration at IRU Comparing Flight Data with MLE Model

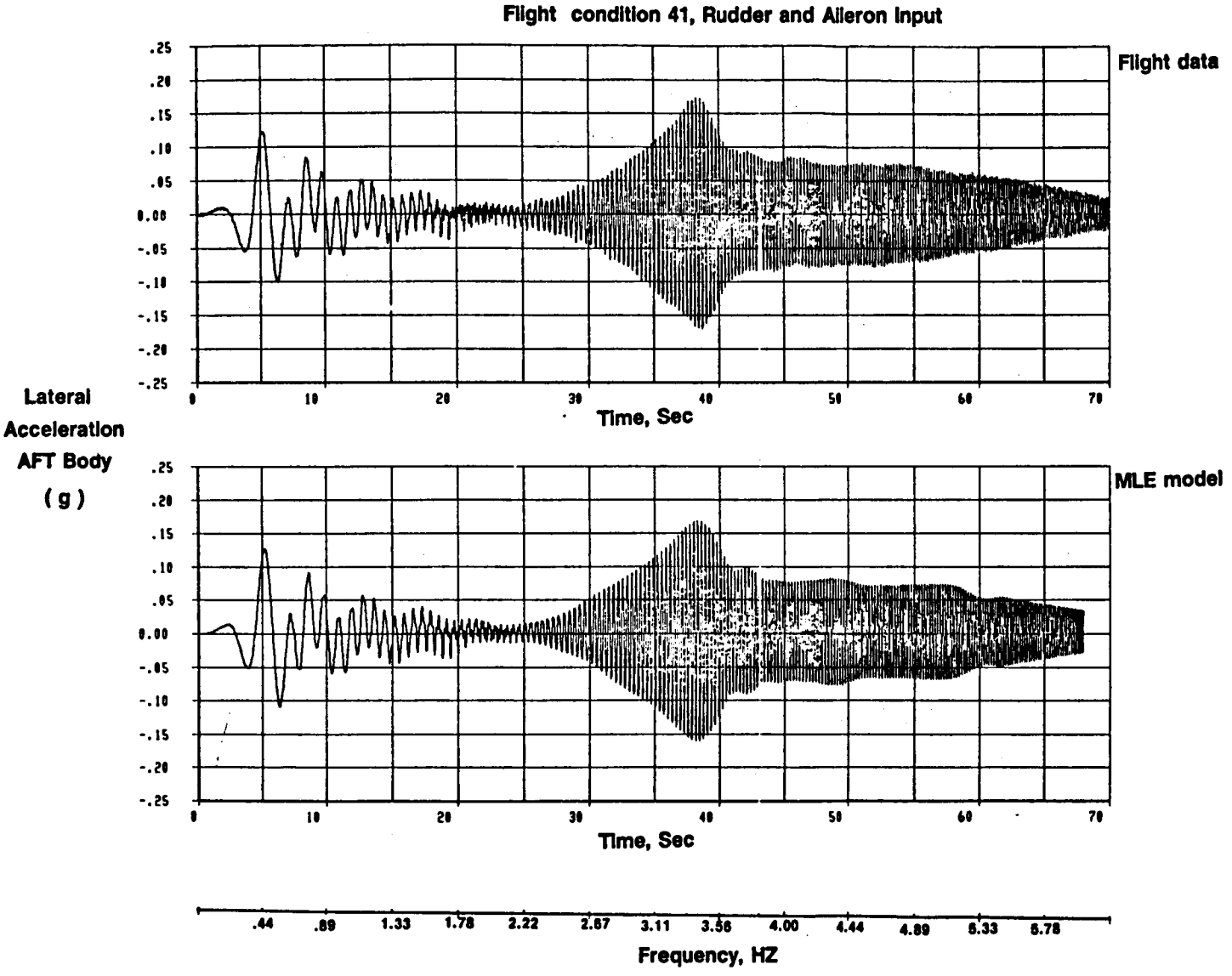

Figure 18. Time Response of Lateral Acceleration at AFT Body Comparing Flight Data with MLE Model

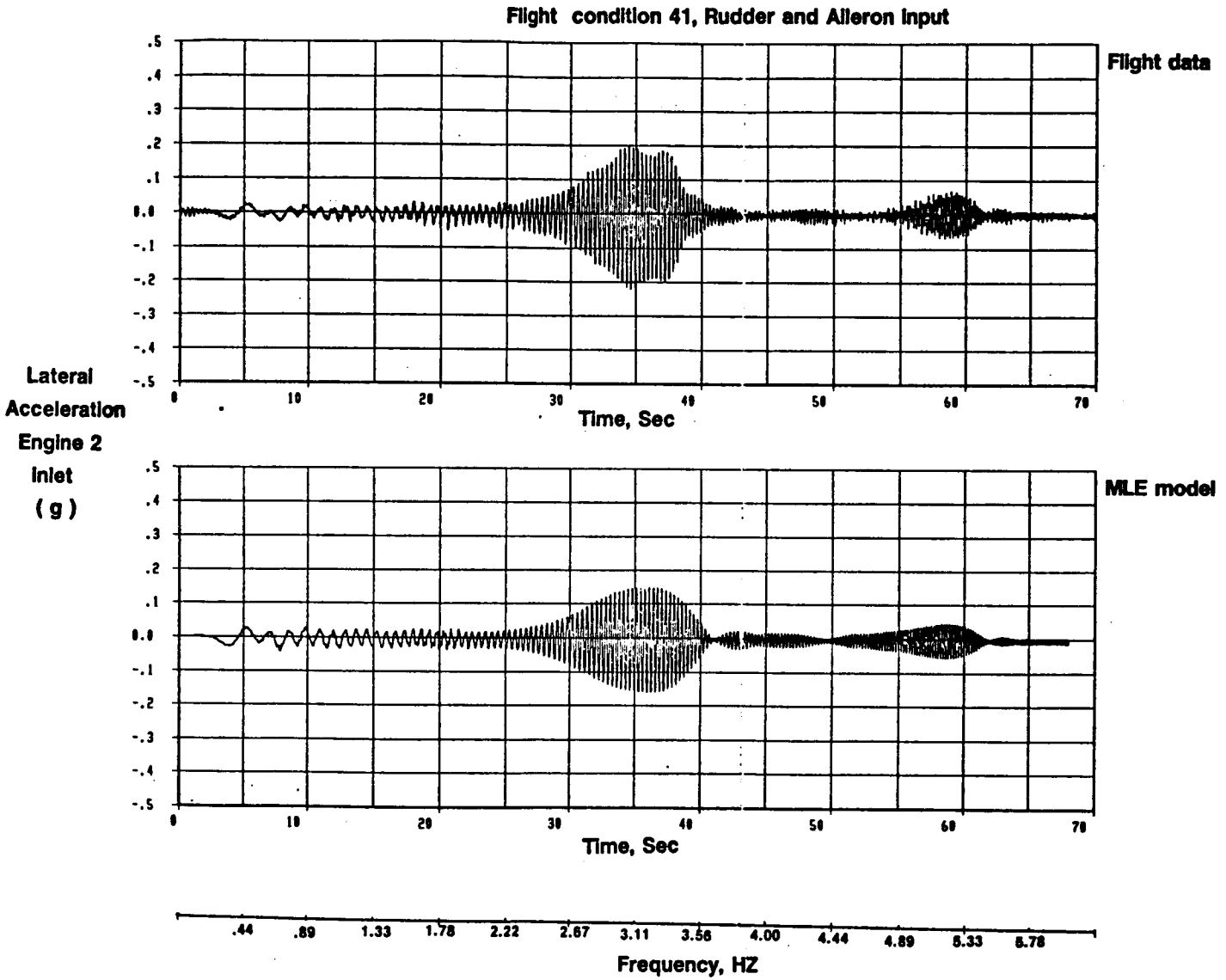

Figure 19. Time Response of Lateral Acceleration at Engine Comparing Flight Data with MLE Model

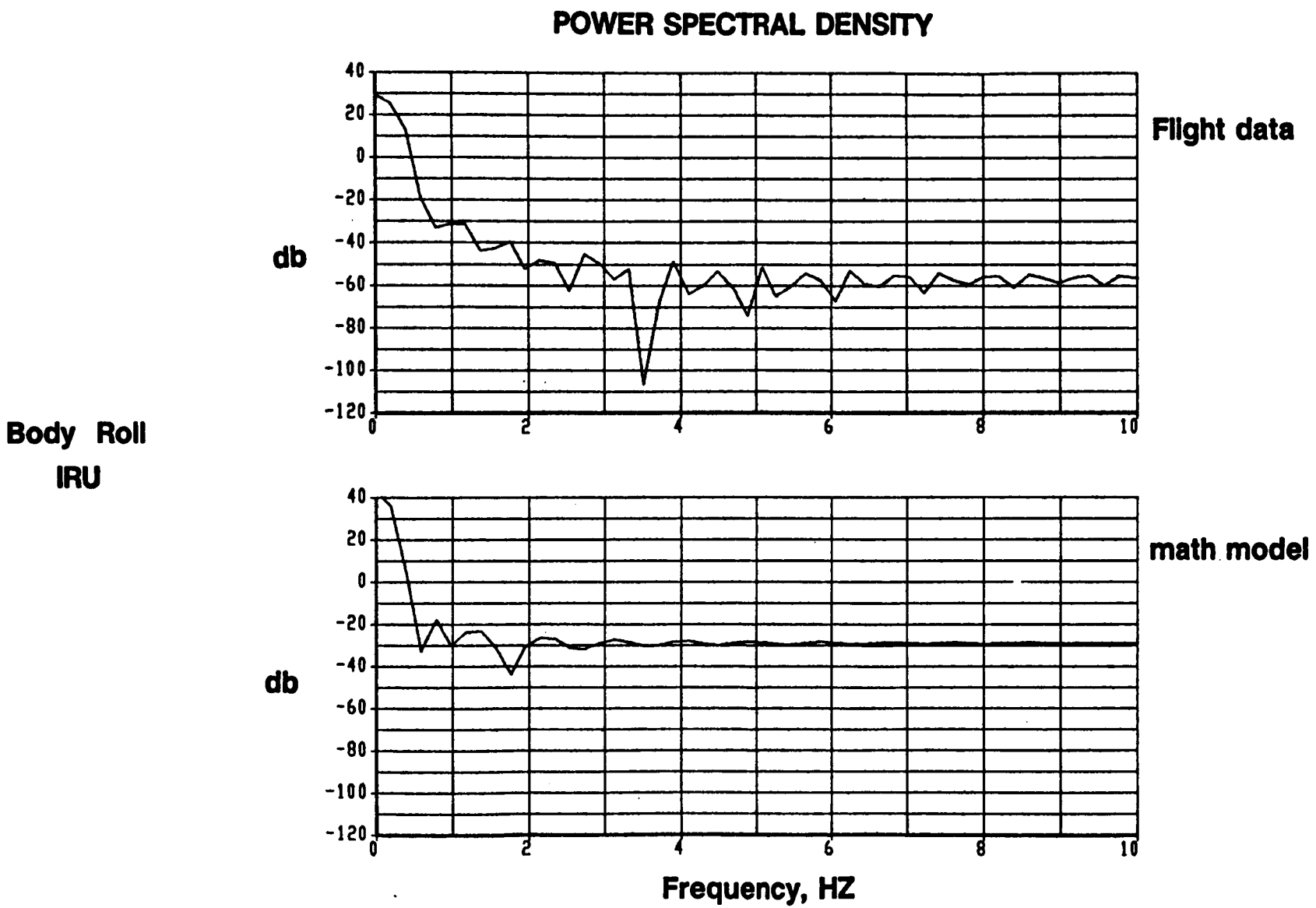

Figure 20. Power Spectral Density Response of Body Roll at IRU Comparing Flight Data with Math Model

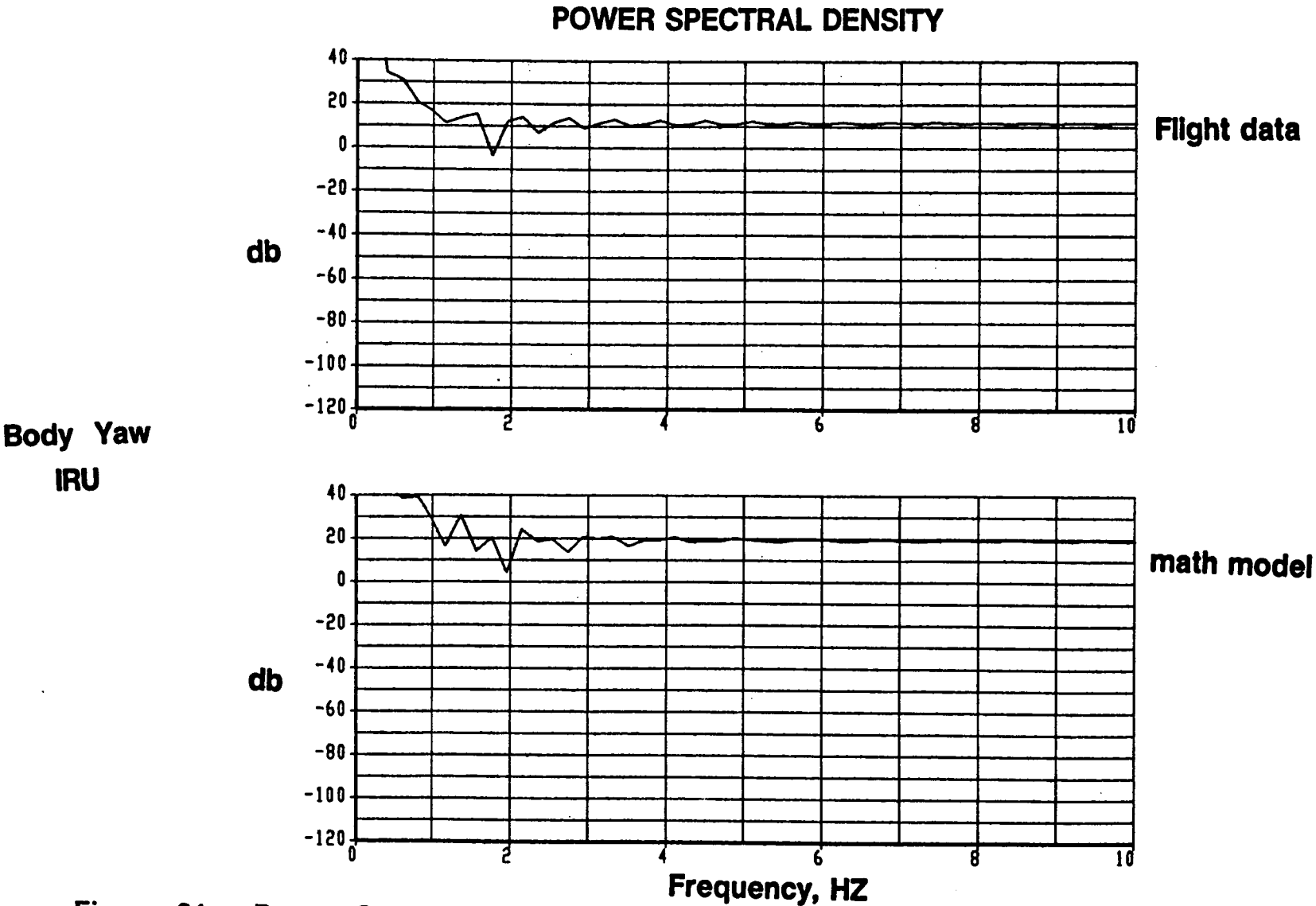

Figure 21. Power Spectral Density Response of Body Yaw at IRU Comparing Flight Data with Math Model

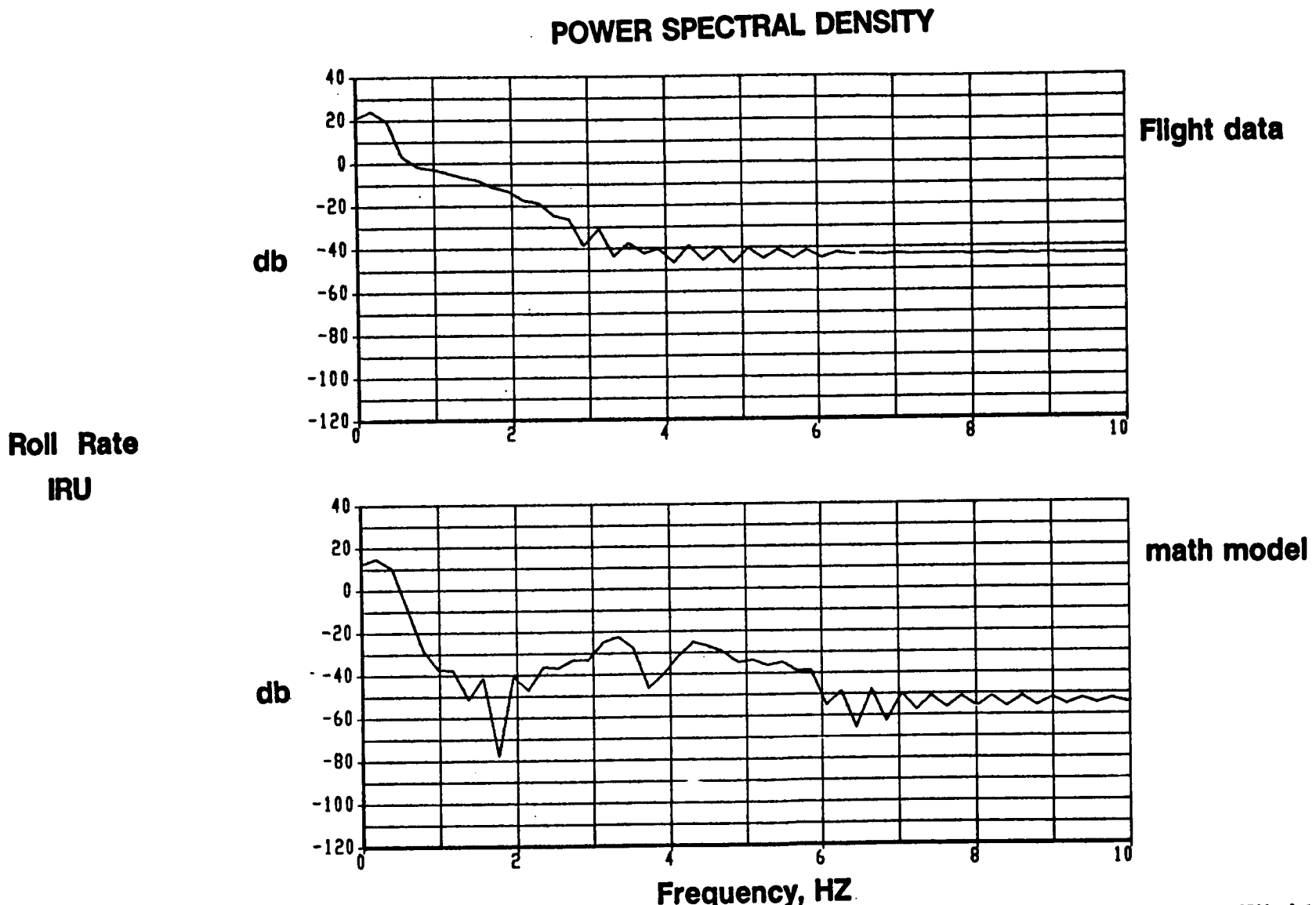

Figure 22. Power Spectral Density Response of Roll Rate at IRU Comparing Flight Data with Math Model

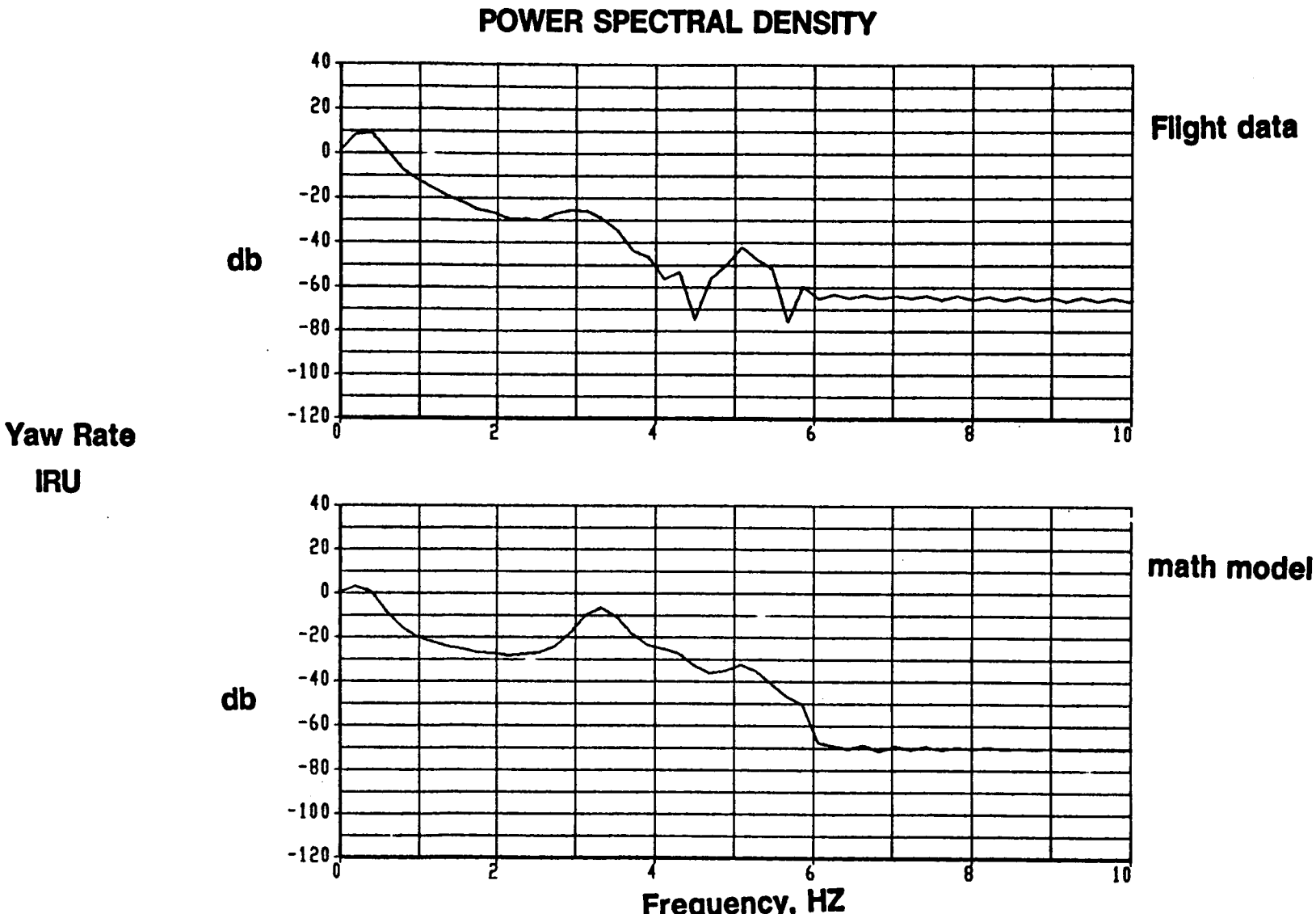

Figure 23. Power Spectral Density Response of Yaw Rate at IRU Comparing Flight Data with Math Model

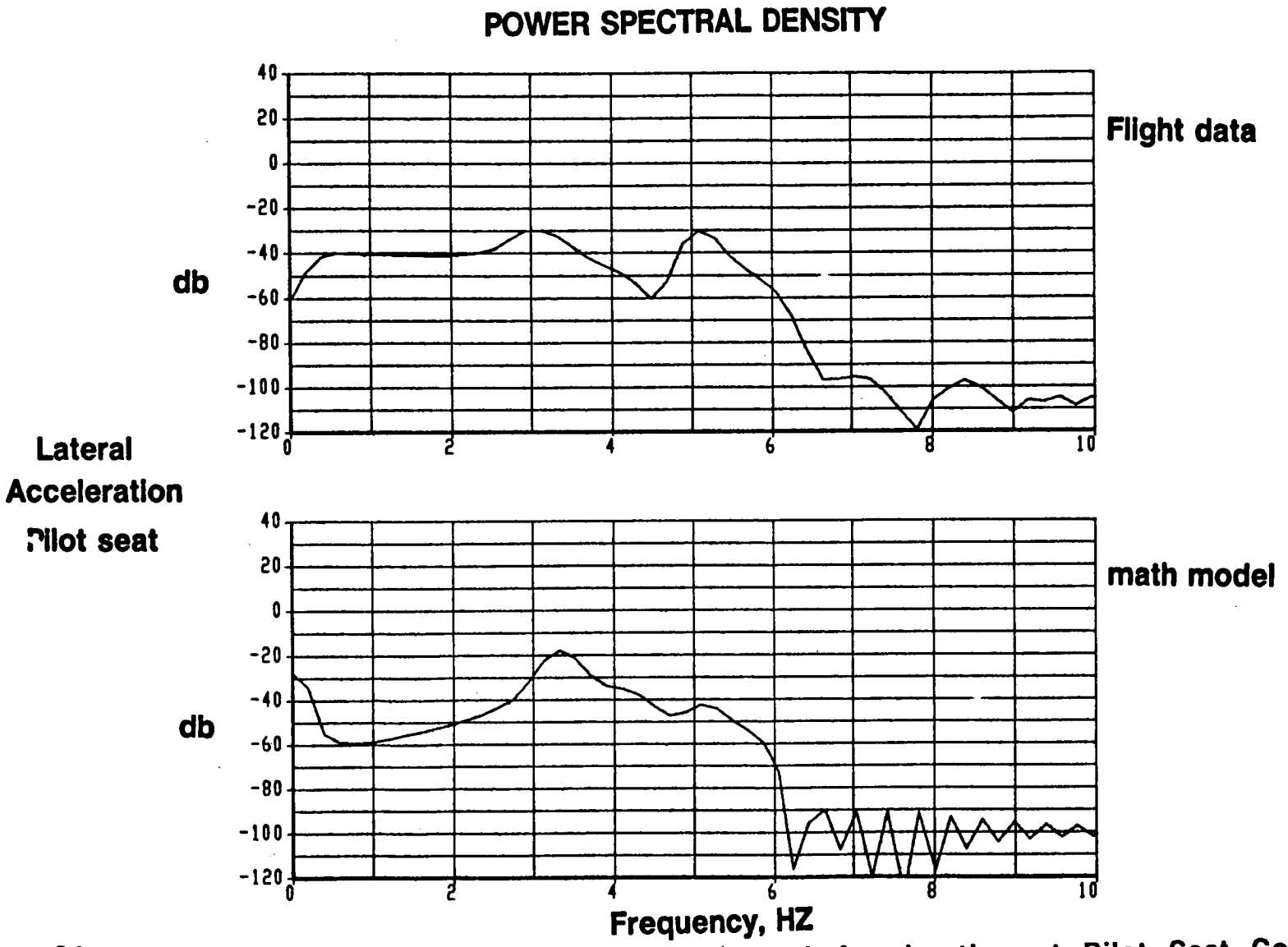

819

Figure 24. Power Spectral Density Response of Lateral Acceleration at Pilot Seat Comparing Flight Data with Math Model

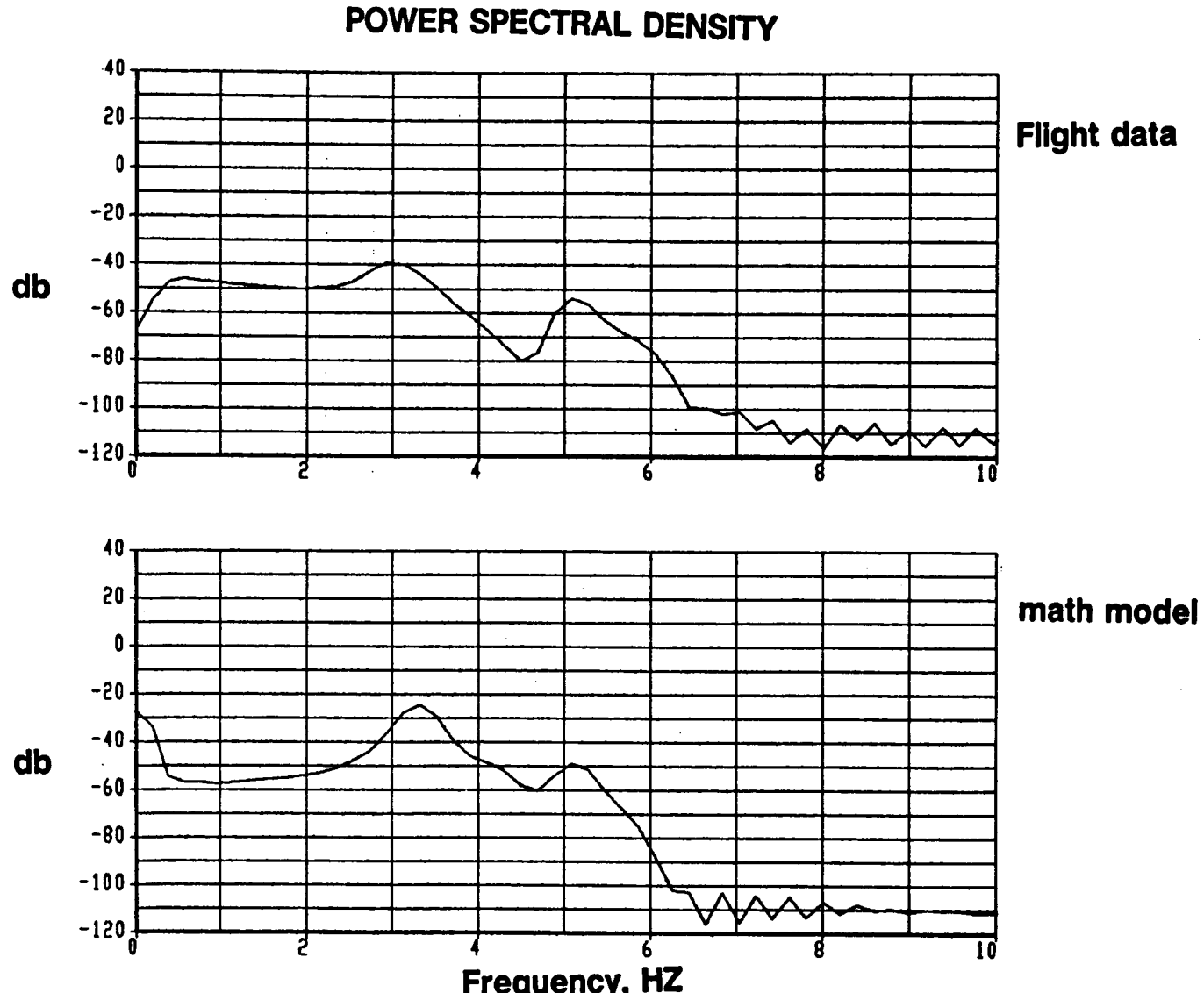

Figure 25. Power Spectral Density Response of Lateral Acceleration at IRU Comparing Flight Data with Math Model

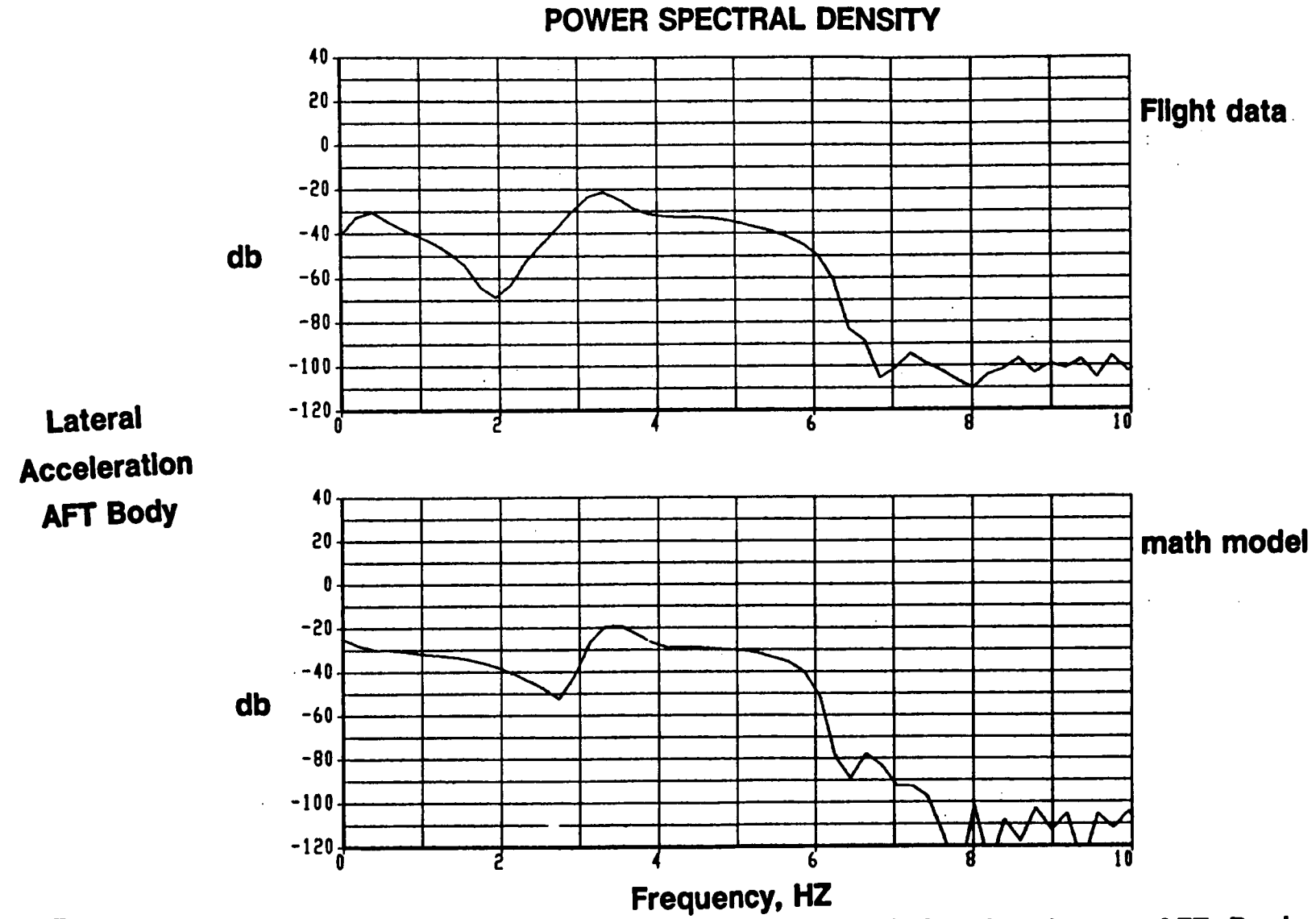

Figure 26. Power Spectral Density Response of Lateral Acceleration at AFT Body Comparing Flight Data with Math Model

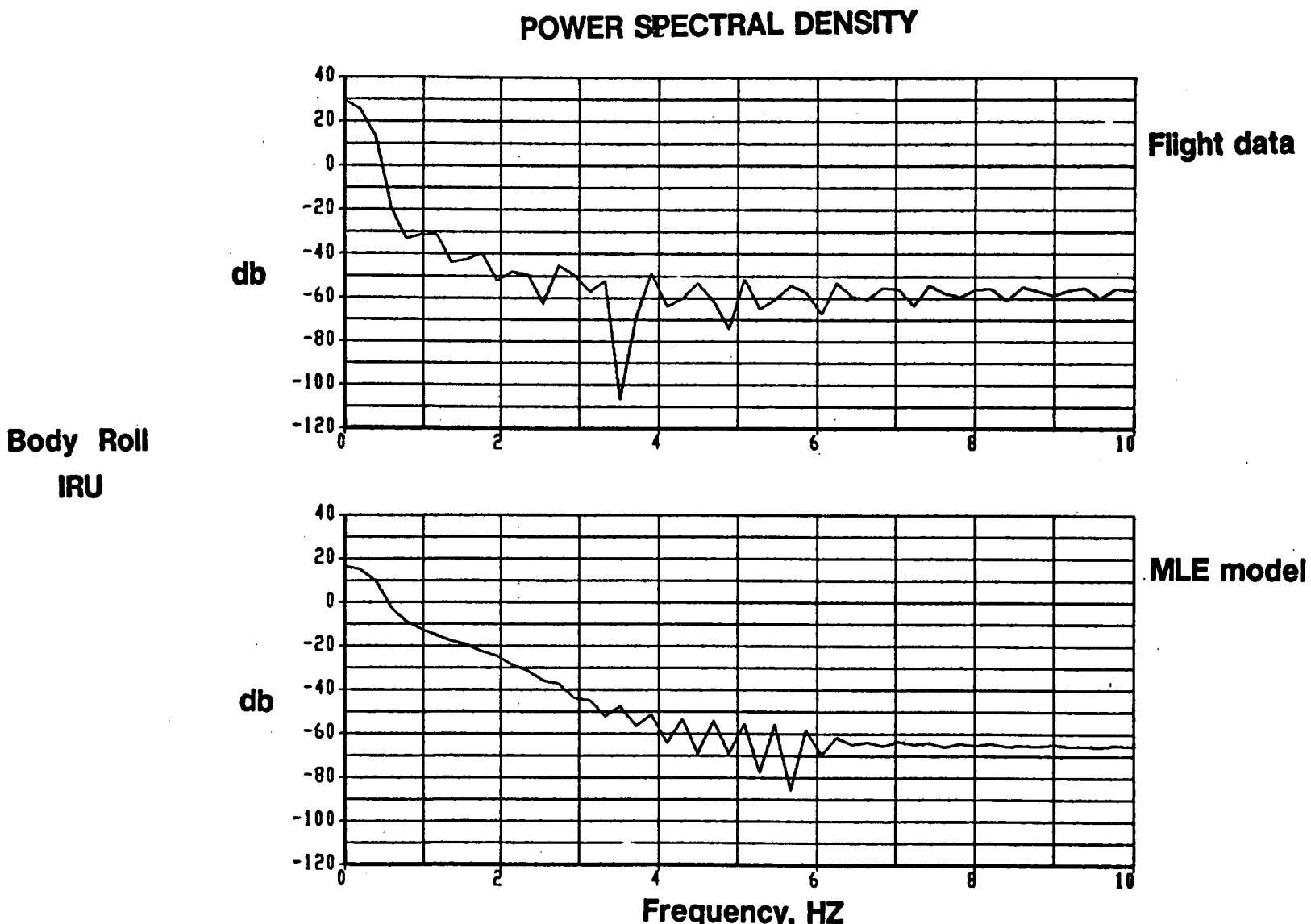

Figure 27. Power Spectral Density Response of Body Roll at IRU Comparing Flight Data with MLE Model

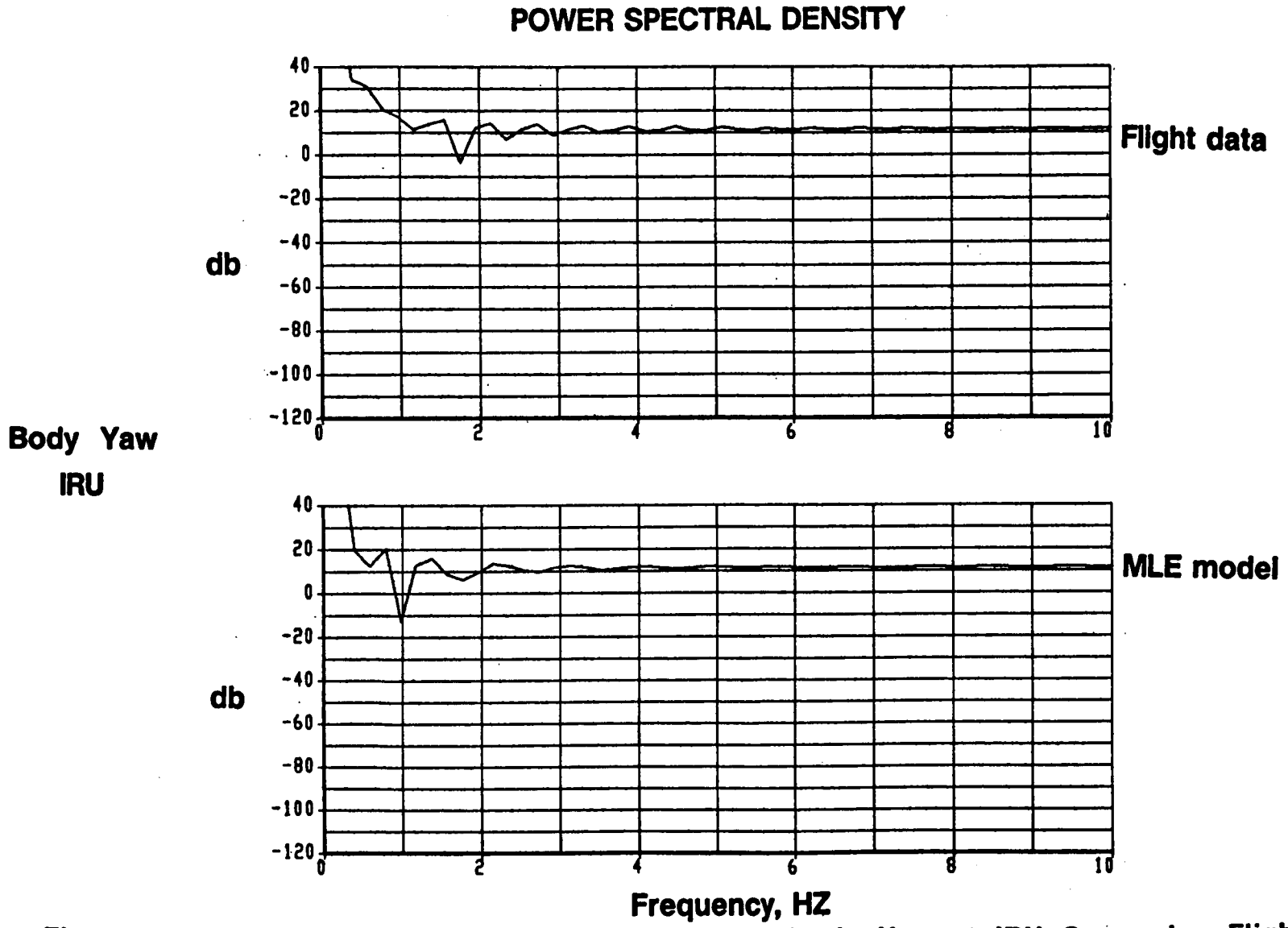

Figure 28. Power Spectral Density Response of Body Yaw at IRU Comparing Flight Data with MLE Model

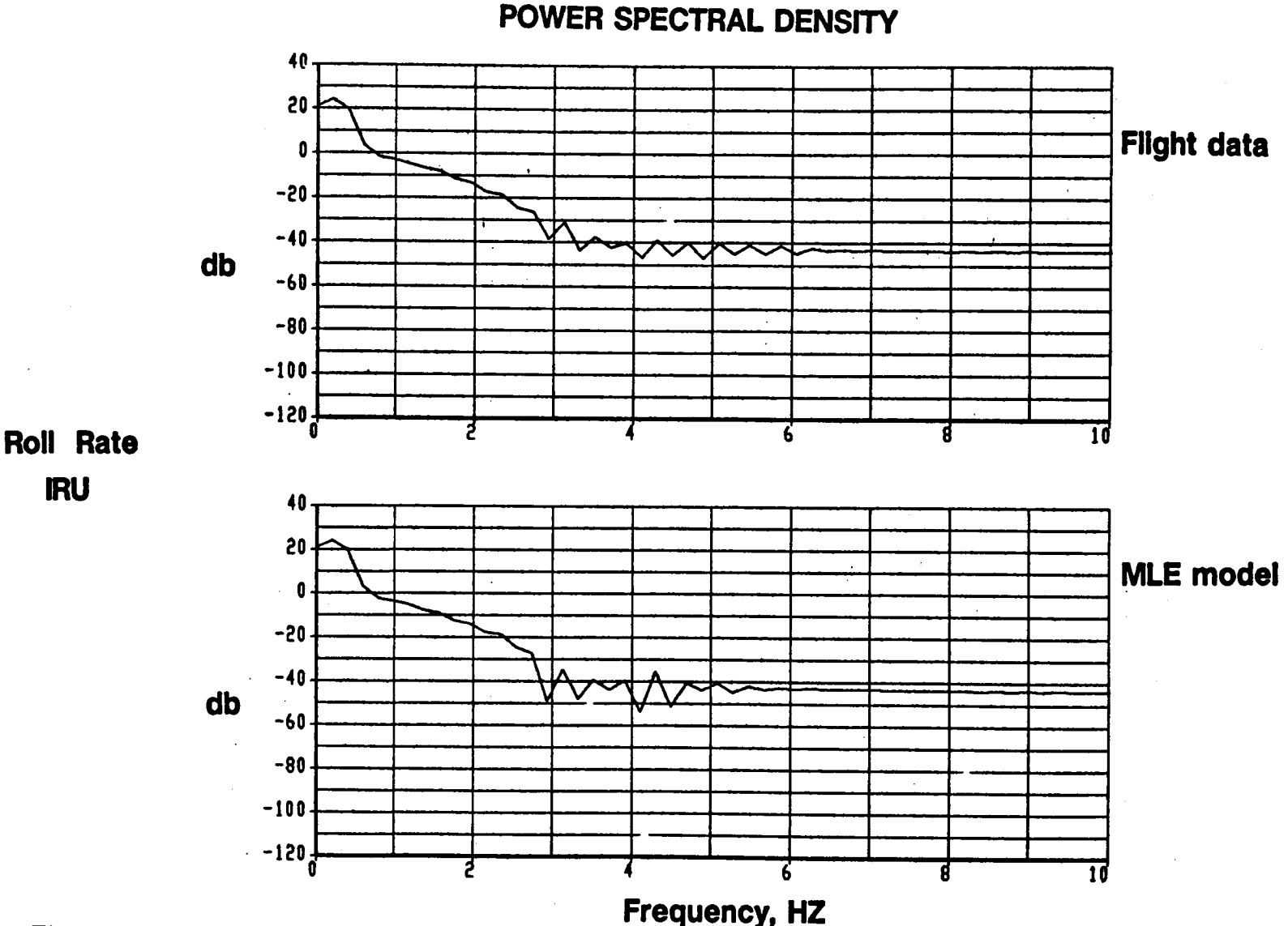

Figure 29. Power Spectral Density Response of Roll Rate at IRU Comparing Flight Data with MLE Model

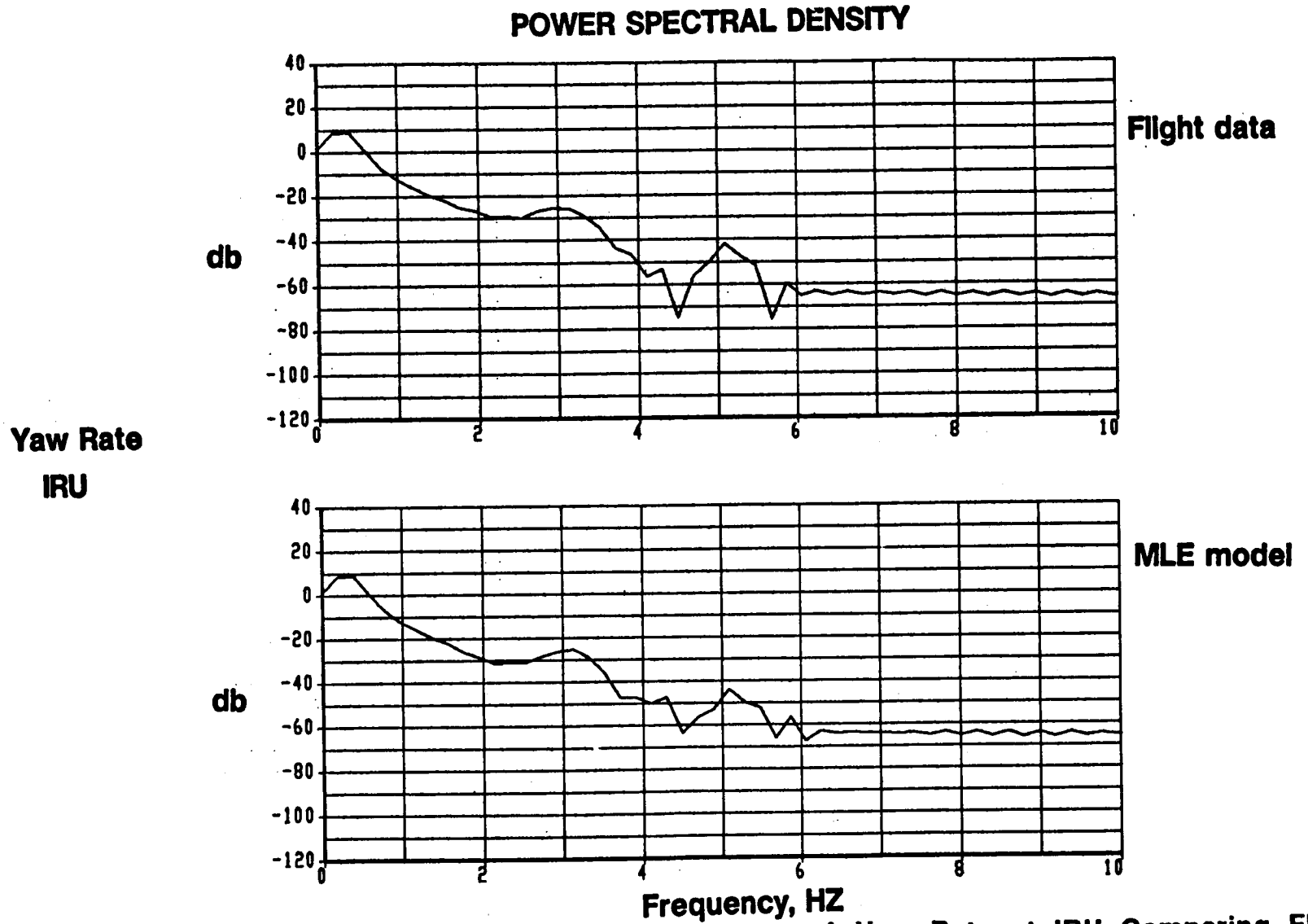

Figure 30. Power Spectral Density Response of Yaw Rate at IRU Comparing Flight Data with MLE Model

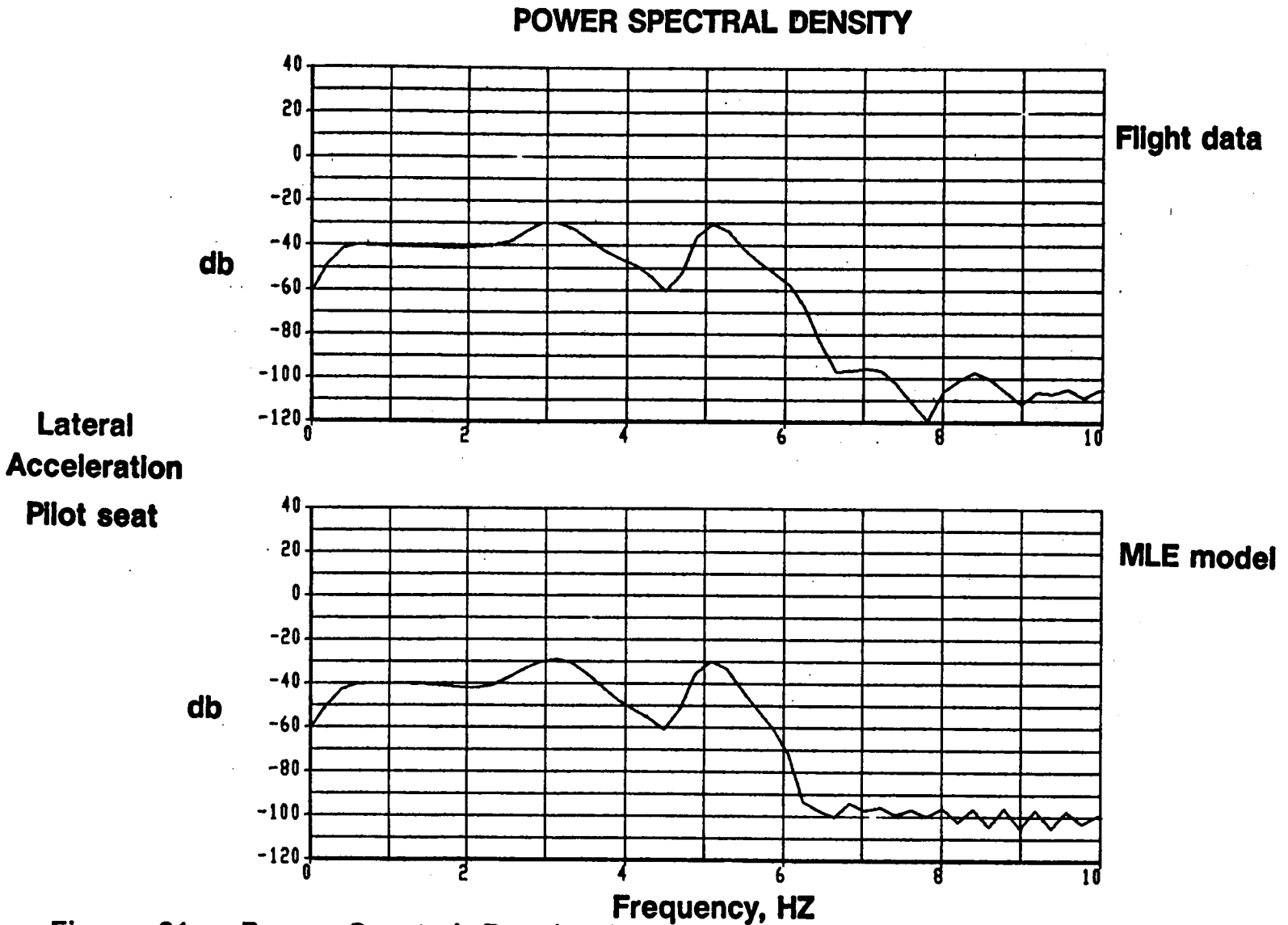

Figure 31. Power Spectral Density Response of Lateral Acceleration at Pilot Seat Comparing Flight Data with MLE Model

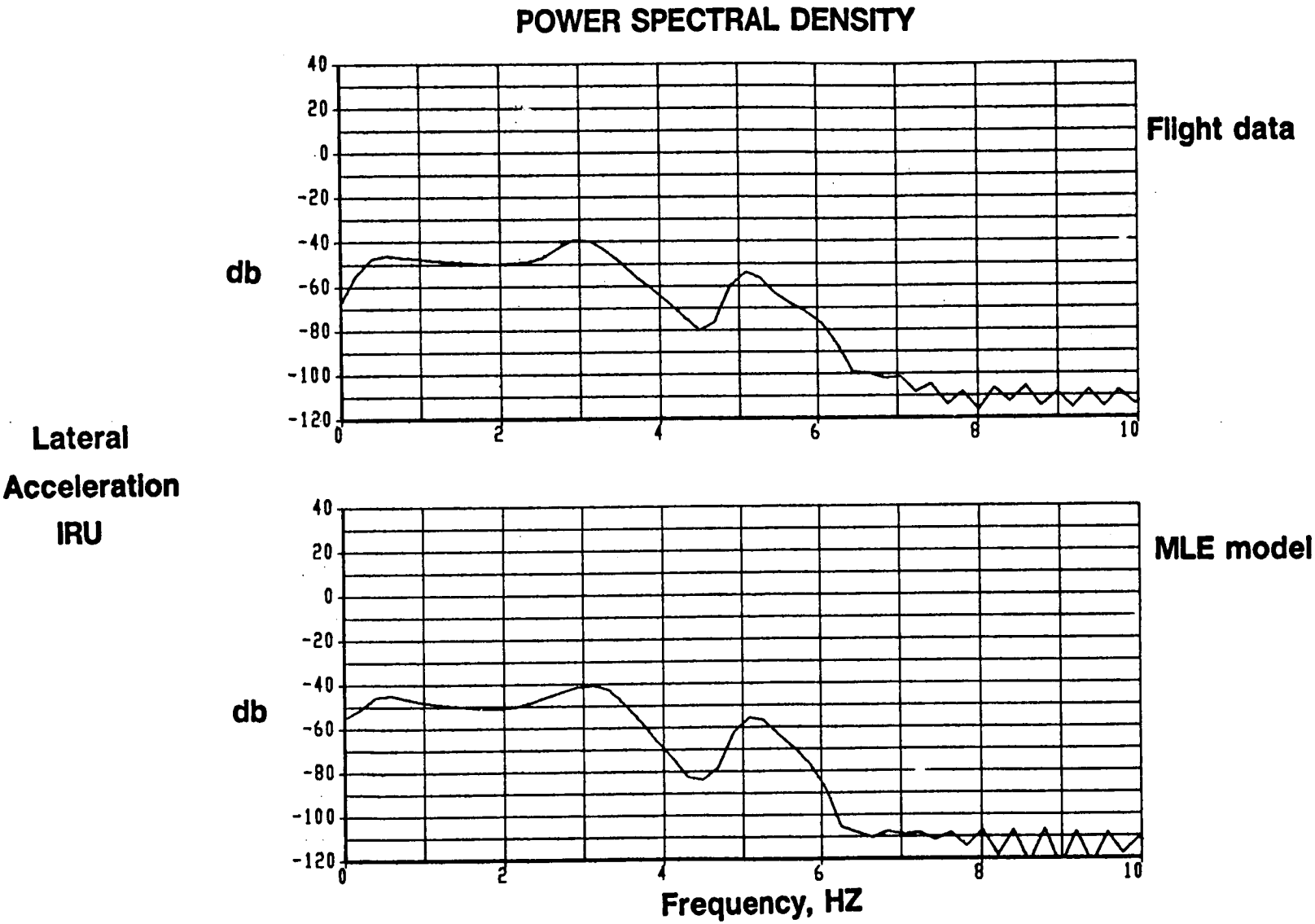

Figure 32. Power Spectral Density Response of Lateral Acceleration at IRU Comparing Flight Data with MLE Model

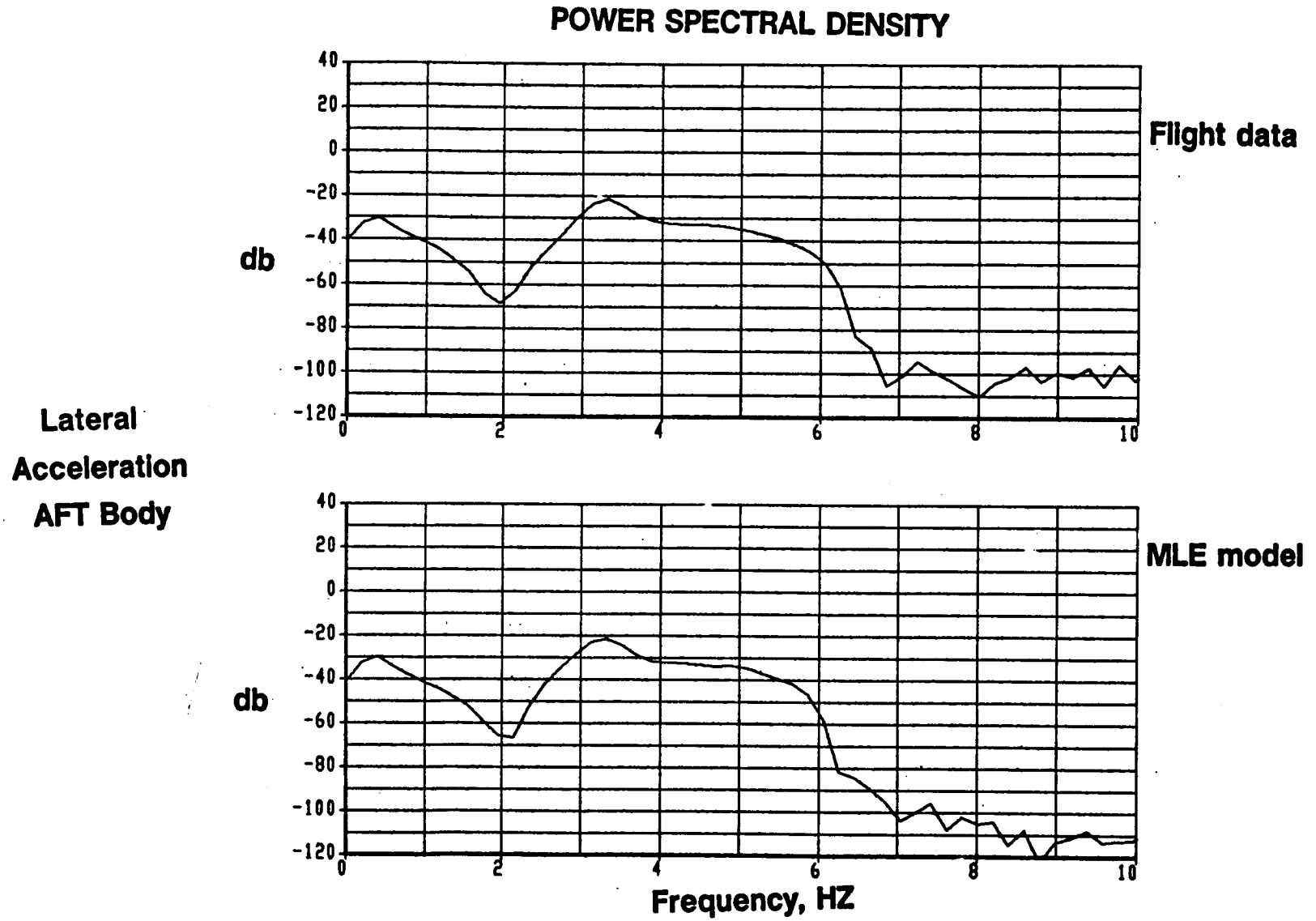

Figure 33. Power Spectral Density Response of Lateral Acceleration at AFT Body Comparing Flight Data with MLE Model

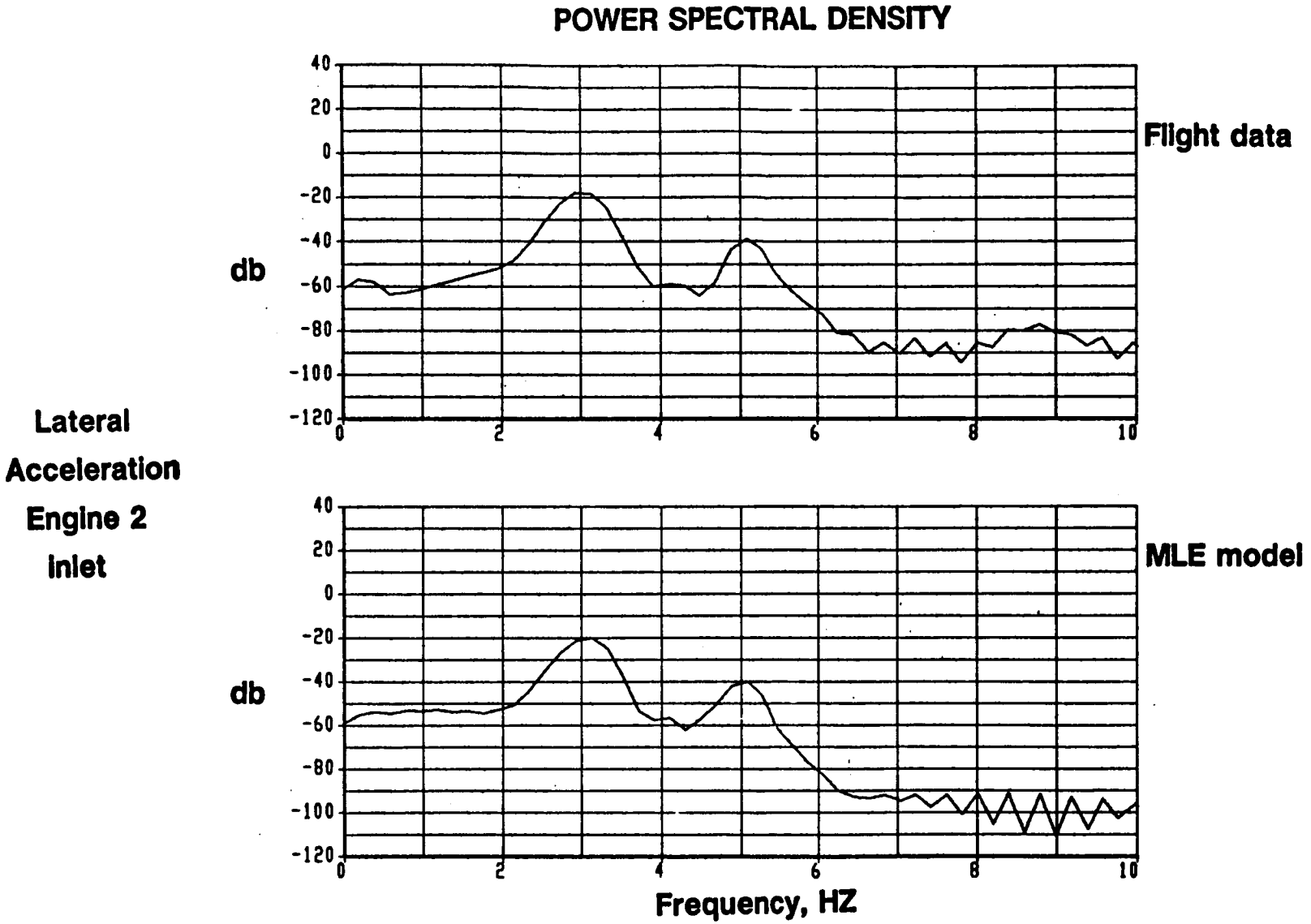

Figure 34. Power Spectral Density of Lateral Acceleration at Engine 2 Inlet Comparing Flight Data with MLE Model

REFERENCES

1. R.E. Maine and K.W. Iliff, "User's Manual for MMLE, a General FORTRAN Program for Maximum Likelihhood Parameter Estimation", NASA Technical Paper 1563, November 1980.

2. G.C. Goodwin and R.L. Payne, "Dynamic System Identification - Experiment Design and Data Analysis", Academic Press, 1977.